HHS Public Access

Author manuscript

Nature. Author manuscript; available in PMC 2018 July 17.

Published in final edited form as:

Nature. 2018 January 25; 553(7689): 461–466. doi:10.1038/nature25451.

αKlotho is a Non-Enzymatic Molecular Scaffold for FGF23 Hormone Signaling

Gaozhi Chen[1,2,#], **Yang Liu**[2,#], **Regina Goetz**[2,†], **Lili Fu**[1,2], **Seetharaman Jayaraman**[3], **Ming-Chang Hu**[4], **Orson W. Moe**[4], **Guang Liang**[1], **Xiaokun Li**[1,*], and **Moosa Mohammadi**[2,*]

[1]Chemical Biology Research Center, School of Pharmaceutical Sciences, Wenzhou Medical University, Wenzhou, Zhejiang 325035, China

[2]Department of Biochemistry & Molecular Pharmacology, New York University School of Medicine, New York, NY 10016, USA

[3]New York Structural Biology Center, New York, NY 10027, USA

[4]Departments of Internal Medicine and Physiology, and Charles and Jane Pak Center of Mineral Metabolism and Clinical Research, University of Texas Southwestern Medical Center, Dallas, TX 75390, USA

Summary

The aging suppressor αKlotho binds to the fibroblast growth factor receptor (FGFR). This commits FGFR to respond to FGF23, a key hormone in the regulation of mineral ion/vitamin D homeostasis. The role and mechanism of this co-receptor are unknown. Here we present the atomic structure of a 1:1:1 ternary complex consisting of the shed extracellular domain of αKlotho, the FGFR1c ligand-binding domain, and FGF23. In this complex, αKlotho simultaneously tethers FGFR1c by its D3 domain and FGF23 by its C-terminal tail, thus implementing FGF23-FGFR1c proximity and conferring stability. The endocrine character of FGF23 notwithstanding, dimerization of the stabilized ternary complexes and receptor activation remain dependent on the binding of heparan sulfate, a mandatory cofactor of paracrine FGF

*To whom correspondence should be addressed: moosa.mohammadi@nyumc.org or xiaokunli@wzmu.edu.cn.
#These authors contributed equally
†Presently self-employed

Competing financial interests

O.W.M. has done paid consultation for AbbVie, Allena, Amgen, and Tricida. He also sits on the board of Klotho Therapeutics. All the other authors have no competing financial interests to declare.

Author contribution statement

G.C. purified and crystallized the ternary complex, analyzed the crystal structure, generated SEC-MALS data (Figures 4a, 5a, b, f), cell-based data (Figure 4), enzyme and thermostability assay data (Figure 2c), and participated in designing experiments and writing/revising the manuscript. Y.L. helped with data collection and analysis of the crystal structure, generated cell-based data (Figure 5), and participated in manuscript revision. R.G. established expression/purification protocols for the ternary complex, performed ternary complex characterization, analyzed mouse data, and participated in editing/revising the manuscript. L.F. generated expression constructs for FGF23, FGFR1c^{ecto}, αKlotho^{ecto} and their structure-based mutated forms, and helped with ternary complex purification. S.J. assisted with diffraction data collection and did excitation/emission scanning of the FGF23-FGFR1c^{ecto}-αKlotho^{ecto} crystal (Extended Data Figure 2c). M-C.H. and O.W.M. generated the mouse data (Extended Data Figures 1c,d and 7a,b). G.L. and X.L. (G.C. and L. F.'s mentors in their home institution, Wenzhou Medical University) participated in manuscript revision. M.M. developed/directed the project, solved/refined/analyzed/interpreted the crystal structure of the ternary complex, and wrote the manuscript.

signaling. The structure of αKlotho is incompatible with its purported glycosidase activity. Thus, shed αKlotho functions as an on-demand non-enzymatic scaffold protein that promotes FGF23 signaling.

Endocrine fibroblast growth factor 23 (FGF23) regulates phosphate and vitamin D homeostasis by reducing cell surface expression of sodium phosphate co-transporters and by repressing transcription of rate-limiting enzymes for vitamin D biosynthesis[1,2] in the kidney. FGF23 exerts its metabolic functions by binding and activating FGF receptor tyrosine kinases (FGFRs)[3] in an αKlotho co-receptor dependent fashion. The extracellular domain of a prototypical FGFR consists of three immunoglobulin-like domains: D1, D2, and D3. The membrane proximal portion comprising D2, D3, and the D2-D3 linker ($FGFR^{ecto}$) is both necessary and sufficient for FGF ligand binding[4,5]. Tissue-specific alternative splicing in the D3 domain of FGFR1-3 generates “b” and “c” isoforms, each with distinct ligand-binding specificity[5,6]. αKlotho, fortuitously discovered as an aging suppressor gene[7], is a single-pass transmembrane protein with an extracellular domain composed of two tandem domains (KL1 and KL2), each with significant homology to family 1 glycosidases[8] (Extended Data Fig. 1a). Membrane-bound αKlotho (αKlotho™) associates with cognate FGFRs of FGF23, namely the “c” splice isoforms of FGFR1 and FGFR3 (FGFR1c and FGFR3c) and FGFR4[9–12]. This enables them to bind and respond to FGF23[9,11,12]. αKlotho™ is predominantly expressed in the kidney distal tubules, the parathyroid gland, and the brain choroid plexus[7,13], and this is considered to determine target tissue specificity of FGF23[11,12]. Cleavage of αKlotho™ by ADAM proteases[14,15] in kidney distal tubules sheds the αKlotho ectodomain ($\alpha Klotho^{ecto}$; Extended Data Fig. 1a) into body fluids, e.g. serum, urine, and cerebrospinal fluid[16–19]. $\alpha Klotho^{ecto}$ is thought to lack co-receptor activity and act as a circulating anti-aging hormone independent of FGF23[20,21]. A plethora of activities has been attributed to shed $\alpha Klotho^{ecto}$, the bulk of which require a purported intrinsic glycosidase activity[22–25].

Here we show that circulating $\alpha Klotho^{ecto}$ is an on-demand *bona fide* co-receptor for FGF23, and determine its crystal structure in complex with $FGFR1c^{ecto}$ and FGF23. The structure reveals that αKlotho serves as a non-enzymatic scaffold that simultaneously tethers FGFR1c and FGF23 to implement FGF23-FGFR1c proximity and hence stability. Surprisingly, heparan sulfate (HS), a mandatory cofactor for paracrine FGFs, is still required as an ancillary cofactor to promote the formation of a symmetric 2:2:2:2 FGF23-FGFR1c-αKlotho-HS quaternary signaling complex.

Soluble $\alpha Klotho^{ecto}$ acts as a co-receptor for FGF23

To determine whether soluble $\alpha Klotho^{ecto}$ can support FGF23 signaling, αKlotho-deficient HEK293 cells – which naturally express FGFRs – were incubated with a concentration of $\alpha Klotho^{ecto}$ sufficient to drive all available cell surface cognate FGFRs into binary complexed form. Following brief rinses with PBS, the cells were stimulated with increasing concentrations of FGF23. In parallel, a HEK293 cell line overexpressing membrane-bound αKlotho (HEK293-αKlotho™) was treated with increasing concentrations of FGF23. The dose-response for FGF23-induced ERK phosphorylation in $\alpha Klotho^{ecto}$-pretreated

untransfected HEK293 cells was similar to that observed in HEK293-αKlotho™ cells (Extended Data Fig. 1b, upper panel), suggesting that αKlotho^{ecto} can serve as a co-receptor for FGF23. Pre-treatment of HEK293-αKlotho™ cells with αKlotho^{ecto} did not result in any further increase in FGF23 signaling, implying that all cell surface FGFRs in this cell line were in binary FGFR-αKlotho™ form (Extended Data Fig. 1b, lower panel). We conclude that soluble and transmembrane forms of αKlotho possess a similar capacity to support FGF23 signaling. Consistent with these results, injection of wild-type mice with αKlotho^{ecto} protein led to an increase in renal phosphate excretion and a decrease in serum phosphate (Extended Data Fig. 1c). Notably, it also led to a 1.5-fold increase in Egr1 transcripts in the kidney (Extended Data Fig. 1d), demonstrating that αKlotho^{ecto} can serve as a *bona fide* co-receptor to support FGF23 signaling in renal proximal tubules. In light of these data, we propose that the pleiotropic anti-aging effects of αKlotho are all dependent on FGF23.

Structural basis for αKlotho co-receptor function

We solved the crystal structure of a human 1:1:1 FGF23-FGFR1c^{ecto}-αKlotho^{ecto} ternary complex at 3.0 Å resolution (Extended Data Table 1). In this complex, αKlotho^{ecto} serves as a massive scaffold, tethering both FGFR1c and FGF23 to itself. In doing so, αKlotho^{ecto} enforces FGF23-FGFR1c proximity and thus augments FGF23-FGFR1c binding affinity (Fig. 1). The overall geometry of the ternary complex is compatible with its formation on the cell surface (Extended Data Fig. 2a).

The binary FGF23-FGFR1c^{ecto} complex adopts a canonical FGF-FGFR complex topology in which FGF23 is bound between the receptor's D2 and D3 domains, engaging both these domains and a short interdomain linker (Extended Data Fig. 3a). However, compared to paracrine FGFs, FGF23 makes fewer/weaker contacts with the D3 domain and D2-D3 linker, explaining the inherently low affinity of FGF23 for FGFR1c (Extended Data Fig. 3b, c). Notably, analysis of the binding interface between FGF23 and FGFR1c D3 in the crystal structure reveals specific contacts between FGF23 and a serine residue uniquely present in the "c" splice isoforms of FGFR1-3 and FGFR4 (Extended Data Fig. 4a). Indeed, replacing this "c"-isoform specific serine residue with a "b"-isoform specific tyrosine impaired FGF23 signaling (Extended Data Fig. 4b, c). We conclude that the FGFR binding specificity inherent to FGF23 operates alongside that of αKlotho (Extended Data Fig. 4d, e) to restrict FGF23 signaling to the "c" splice isoforms and FGFR4[11,12].

In the ternary complex, αKlotho^{ecto} exists in an extended conformation. Consistent with their sequence homology to the glycoside hydrolase A (GH-A) clan[8], αKlotho KL1 (Glu-34 to Phe-506) and KL2 (Leu-515 to Ser-950) domains each assume a $(\beta\alpha)_8$ TIM barrel fold consisting of an inner eight-stranded parallel β-barrel and eight surrounding α-helices (Fig. 2a and Extended Data Fig. 5a). The two KL domains are connected by a short, proline-rich and hence stiff linker (Pro-507 to Pro-514) (Fig. 1a, b). KL1 sits atop KL2, engaging it via a few interdomain contacts involving the N-terminus preceding the β1 strand, the α7 helix of KL1, and the β5α5, β6α6 loops and the α7 helix of KL2 (Extended Data Fig. 2b). Intriguingly, one of the interdomain contacts is mediated by a Zn^{2+} ion (Fig. 3c and Extended Data Fig. 2b, c). These contacts stabilize the observed elongated conformation of αKlotho^{ecto}, creating a deep cleft between the two KL domains. This merges with a wide-

open central β-barrel cavity in KL2, and forms a large binding pocket that tethers the distal C-terminal tail of FGF23 past the ^{176}Arg-His-Thr-Arg^{179} proteolytic cleavage site (Fig. 1b). Meanwhile, the long β1α1 loop of KL2 (Fig. 2a) protrudes as much as 35 Å away from the KL2 core to latch onto the FGFR1c D3 domain, thus anchoring the receptor to αKlotho (Fig. 1b). Accordingly, we have named this KL2 loop the "Receptor Binding Arm" (RBA; residues 530-578; Extended Data Fig. 5a).

We superimposed the TIM barrels of KL1 and KL2 onto that of Klotho Related Protein (KLrP; also known as GBA3), the cytosolic member of the Klotho family with proven glycosylceramidase activity[26]. This comparison revealed major conformational differences in the loops surrounding the entrance to the catalytic pocket in KL1 and KL2 (Fig. 2b and Extended Data Fig. 5b–d). Moreover, both KL domains lack one of the key catalytic glutamates deep within the putative catalytic pocket. These substantial differences are incompatible with an intrinsic glycosidase activity for αKlotho[22,23]. Indeed, αKlotho^{ecto} failed to hydrolyze substrates for both sialidase and β-glucuronidase *in vitro* (Fig. 2c). Together, our data define αKlotho as the only known example of a TIM barrel protein that serves purely as a non-enzymatic molecular scaffold.

Binding interface between αKlotho and FGFR1c

The interface between αKlotho RBA and FGFR1c D3 (Fig. 3a) buries over 2,200 Å^2 of solvent-exposed surface area, which is consistent with the high affinity of αKlotho binding to FGFR1c (K_D = 72 nM)[10]. At the distal tip of the RBA, residues ^{547}Tyr-Leu-Trp^{549} and ^{556}Ile-Leu-Arg^{558} form a short β-strand pair (RBA-β1:RBA-β2) as their hydrophobic side chains are immersed in a wide hydrophobic groove between the four-stranded βC'-βC-βF-βG sheet and the βC-βC' loop of FGFR1c D3 (Fig. 3b, upper panel). The RBA-β1:RBA-β2 strand pair forms an extended β sheet with the βC'-βC-βF-βG sheet of D3 as the backbone atoms of RBA-β1 and D3 βC' make three hydrogen bonds which further augment the interface (Fig. 3b, lower panel). Residues at the proximal end of the RBA engage a second smaller binding pocket at the bottom edge of D3 next to the hydrophobic groove (Extended Data Fig. 6a, b). Both αKlotho binding pockets in the receptor D3 domain differ between "b" and "c" splice isoforms. Leu-342, for example, is strictly conserved in the "c" splice isoforms of FGFR1-3 and FGFR4. This explains the previously described binding selectivity of αKlotho for this subset of FGFRs (Extended Data Fig. 4a)[11,12,27].

Consistent with the crystal structure, soluble αKlotho lacking the RBA (αKlotho$^{ecto/\Delta RBA}$) failed to form a binary complex with FGFR1c^{ecto} in solution (Fig. 4a) and hence could not support FGF23 signaling (Fig. 4b). Likewise, membrane-bound αKlotho lacking the RBA (αKlotho$^{TM/\Delta RBA}$) was also disabled in acting as a FGF23 co-receptor (Fig. 4b). Importantly, αKlotho$^{ecto/\Delta RBA}$ did not exhibit any phosphaturic activity *in vivo* (Extended Data Fig. 7a). On the contrary, the αKlotho$^{ecto/\Delta RBA}$ mutant antagonized the activity of native αKlotho by sequestering FGF23 into functionally inactive binary complexes, i.e. by acting as an FGF23 ligand trap (Extended Data Fig. 7). These data refute the concept that αKlotho^{ecto} functions as an FGF23-independent phosphaturic enzyme[24]. Our conclusion is supported by a gene knockout study which compared the phenotypes of *Fgf23*$^{-/-}$, *Klotho*$^{-/-}$, and *Fgf23*$^{-/-}$/*Klotho*$^{-/-}$ mice[28].

Binding interface between αKlotho and FGF23

Regions from both KL domains act together to recruit FGF23 (Fig. 1b), thus explaining why only an intact αKlotho ectodomain is capable of supporting FGF23 signaling[12,29]. The interactions between FGF23 and αKlotho result in the burial of a large amount of solvent-exposed surface area (2,732 Å^2), of which nearly two-thirds (1961 Å^2) are buried between the FGF23 C-terminal tail and αKlotho, with the remaining one-third buried between the FGF23 core and αKlotho (Fig. 3a). At the interface between αKlotho and FGF23 C-terminal tail, FGF23 residues ^{188}Asp-Pro-Leu-Asn-Val-Leu^{193} adopt an unusual cage-like conformation (Fig. 3a, c) which is tethered by residues from both KL domains via hydrogen bonds and hydrophobic contacts deep inside the KL1-KL2 cleft (Fig. 3c). Further downstream, the side chains of Lys-194, Arg-196, and Arg-198 of the FGF23 C-terminal tail dip into the central barrel cavity of KL2, making hydrogen bonds with multiple αKlotho residues (Fig. 3c). At the interface between the FGF23 β-trefoil core and αKlotho, residues from the β5–β6 turn and the αC helix of FGF23 make hydrogen bonds and hydrophobic contacts with residues in the short β7-α7 and β8-α8 loops at the upper rim of the KL2 cavity (Extended Data Fig. 6a, c).

To test the biological relevance of the observed contacts between αKlotho and FGF23 C-terminal tail, we introduced multiple mutations into αKlotho™ and FGF23 in order to disrupt αKlotho-FGF23 binding (Fig. 4c). Consistent with our structure-based predictions, all αKlotho™ mutants showed an impaired ability to support FGF23 signaling (Fig. 4c). The FGF23 mutants also exhibited a reduced ability to signal, regardless of whether soluble or membrane-bound αKlotho served as co-receptor (Fig. 4d). Remarkably, the FGF23^{D188A} mutant (which eliminates the intramolecular hydrogen bonds that support cage conformation) was totally inactive, underscoring the importance of the cage-like conformation in the tethering of FGF23 to αKlotho. Notably, tethering of this cage-like structure requires a precise alignment of residues from both KL domains deep within the KL1-KL2 cleft (Fig. 3c), implying that their correct apposition is critically important for αKlotho co-receptor activity. These structural observations suggest that the bound Zn^{2+} ion serves as a prosthetic group in αKlotho by minimizing interdomain flexibility and hence promoting co-receptor activity. Consistent with such a role, mutants of membrane-anchored αKlotho™ carrying alanine in place of two, three, or all four Zn^{2+} coordinating amino acids (Fig. 3c) showed a reduced ability to support FGF23 signaling (Fig. 4e). Together with our data on the impact of RBA deletion, these results corroborate the biological relevance of the crystallographically-deduced mode by which αKlotho implements FGF23-FGFR1c proximity and thus confers high binding affinity.

FGF23 signaling is αKlotho and HS-dependent

Both FGF23 and FGFR1c have a measurable (albeit weak) binding affinity for HS. Because HS is ubiquitously expressed, we wondered whether it participates in the apparent αKlotho^{ecto}-mediated FGF23-FGFR dimerization in our cell-based and *in vivo* experiments. We therefore analyzed the molecular mass of the ternary complex in the absence and presence of increasing molar equivalents of homogenously sulfated heparin hexasaccharide (HS6). Consistent with our previous observations, in the absence of HS6, the ternary

complex migrated as a monomeric species[10] with an apparent molecular mass of 150 kDa, in good agreement with the theoretical value for a 1:1:1 complex (160 kDa) (Fig. 5a). With increasing molar ratios of HS6 to ternary complex, the peak for monomeric ternary complex diminished, while a new peak with a molecular mass of 300 kDa (corresponding to a 2:2:2 FGF23-FGFR1c^{ecto}-αKlotho^{ecto} dimer) appeared and increased in prominence. Excess HS6 beyond a 1:1 molar ratio of HS6 to ternary complex did not lead to any further increase in the amount of dimer complex formed, as judged by the integrated area of the dimer complex peak (Fig. 5a). We conclude that HS is required for the dimerization of 1:1:1 FGF23-FGFR1c^{ecto}-αKlotho^{ecto} complexes, and that at least a 1:1 molar ratio of HS6 to ternary complex is required for complete dimerization of the complex in solution (Fig. 5a). To further confirm the HS-dependency of dimerization, we introduced mutations into the HS-binding sites of FGFR1c (K160Q/K163Q, FGFR1c$^{\Delta HBS}$, and K207Q/R209Q, FGFR1c$^{\Delta HBS'}$) and FGF23 (R140A/R143A; FGF23$^{\Delta HBS}$). Neither mutating the HS-binding site in FGFR1c nor mutating that site in FGF23 impacted the formation of a monomeric 1:1:1 FGF23-FGFR1c-αKlotho complex in solution, demonstrating that αKlotho-mediated stabilization of the FGF23-FGFR complex is HS-independent. However, ternary complexes containing any of these three mutants failed to dimerize in the presence of HS6 (Fig. 5b).

Reconstitution experiments in the context of BaF3 cells (an FGFR, αKlotho, and HS triple deficient cell line[30]) showed that both soluble αKlotho^{ecto} and membrane-bound αKlotho™ required HS to support FGF23-mediated FGFR1c activation in a more physiological context (Fig. 5c). We also examined the impact of the HS-binding site mutations in FGFR1c and FGF23 on FGFR1c activation by FGF23 in BaF3 cells (Fig. 5d). In agreement with our solution binding data, activation by FGF23 of HS-binding site mutants of FGFR1c in BaF3 cells was markedly impaired, regardless of whether soluble or membrane-bound αKlotho served as the co-receptor (Fig. 5d). Similarly, the HS-binding site mutant of FGF23 showed a significantly reduced ability to activate FGFR1c (Fig. 5e). These *in vitro* and cell-based analyses unequivocally demonstrate that whereas HS fulfills a dual role in paracrine FGF signaling – enhancing 1:1 FGF-FGFR binding and promoting 2:2 FGF-FGFR dimerization – it shares this task with αKlotho in FGF23 signaling. Thus, αKlotho primarily acts to promote 1:1 FGF23-FGFR1c binding, whereas HS induces dimerization of the resulting FGF23-FGFR1c-αKlotho complexes.

Based on the crystallographically-deduced 2:2:2 (PDB ID: 1FQ9)[4] and 2:2:1 (PDB ID: 1E0O)[31] paracrine FGF-FGFR-HS dimerization models, two distinct HS-induced 2:2:2 endocrine FGF23-FGFR1c-αKlotho quaternary dimers can be envisioned that differ dramatically in the composition of the dimer interface (Extended Data Fig. 8). Specifically, in the 2:2:2:1 model, there would be no protein-protein contacts between the two 1:1:1 FGF-FGFR-αKlotho protomers (Extended Data Fig. 8a). By contrast, in the 2:2:2:2 model, FGF23 and FGFR from one 1:1:1 FGF-FGFR-αKlotho protomer would interact with the D2 domain of FGFR in the adjacent 1:1:1 FGF-FGFR-αKlotho protomer across a two-fold dimer interface (Extended Data Fig. 8b). Based on the fundamental differences in the composition of the dimer interface between these two models, we introduced mutations into the secondary-receptor-binding site (SRBS) in FGF23 (M149A/N150A/P151A; FGF23$^{\Delta SRBS}$) and into the corresponding secondary-ligand-binding site (SLBS) in FGFR1c D2 (I203E, FGFR1c$^{\Delta SLBS}$, and V221D, FGFR1c$^{\Delta SLBS'}$), both of which are unique to the

2:2:2:2 quaternary dimer model. The direct receptor-receptor binding site in FGFR1c D2 (A171D; FGFR1c$^{\Delta RRBS}$), another binding site unique to the 2:2:2:2 model, was also mutated (Extended Data Fig. 8b). While all these FGF23 and FGFR1c mutants were able to form ternary complexes with αKlotho^{ecto}, the ternary complexes containing any of the mutated proteins were impaired in their ability to dimerize in the presence of HS6 in solution (Fig. 5f). Moreover, FGF23$^{\Delta SRBS}$ mutant showed a markedly diminished ability to activate FGFR1c in BaF3 cells (Fig. 5e). The loss-of-function effects of these mutations are consistent with a 2:2:2:2 quaternary dimer model (Extended Data Fig. 8b). Hence, we envision that HS engages the HS-binding sites of FGFR1c and FGF23 in two stabilized 1:1:1 FGF23-FGFR1c-αKlotho ternary complexes to promote the formation of a two-fold symmetric 2:2:2:2 FGF23-FGFR1c-αKlotho-HS dimer (Fig. 5g). In doing so, HS enhances reciprocal interactions of FGFR1c D2 and FGF23 from one ternary complex with FGFR1c D2 in the other ternary complex, thereby buttressing the dimer (Extended Data Fig. 8b). This replicates the role that HS plays in paracrine FGF signaling[4]. In contrast to HS, αKlotho molecules do not directly participate in the dimer interface (Fig. 5g), but rather indirectly support HS-induced dimerization by enhancing 1:1 FGF23-FGFR1c binding affinity. Hence, it appears that FGF23 strikes a fine balance between losing a large amount of HS-binding affinity to enable its endocrine mode of action and retaining sufficient HS-binding affinity to allow HS-mediated dimerization of two 1:1:1 FGF23-FGFR1c-αKlotho complexes. These considerations do not formally exclude the possibility that 2:2:2:2 and 2:2:2:1 quaternary dimers might co-exist as a higher order cluster on the cell surface, as has been proposed for paracrine 2:2:2 and 2:2:1 FGF-FGFR1-HS dimers[32].

FGF19 and FGF21, the other two endocrine FGFs, require βKlotho as an obligate co-receptor to bind and activate cognate FGFRs[33,34] so as to mediate effects that regulate, for example, metabolic pathways involved in bile acid biosynthesis or fatty acid oxidation[35,36]. Based on the structural analysis and supporting cell-based data shown in Extended Data Fig. 9 and 10, we propose that βKlotho, similar to αKlotho, functions as a non-enzymatic molecular scaffold to promote signaling by these two FGF hormones.

Extended Data

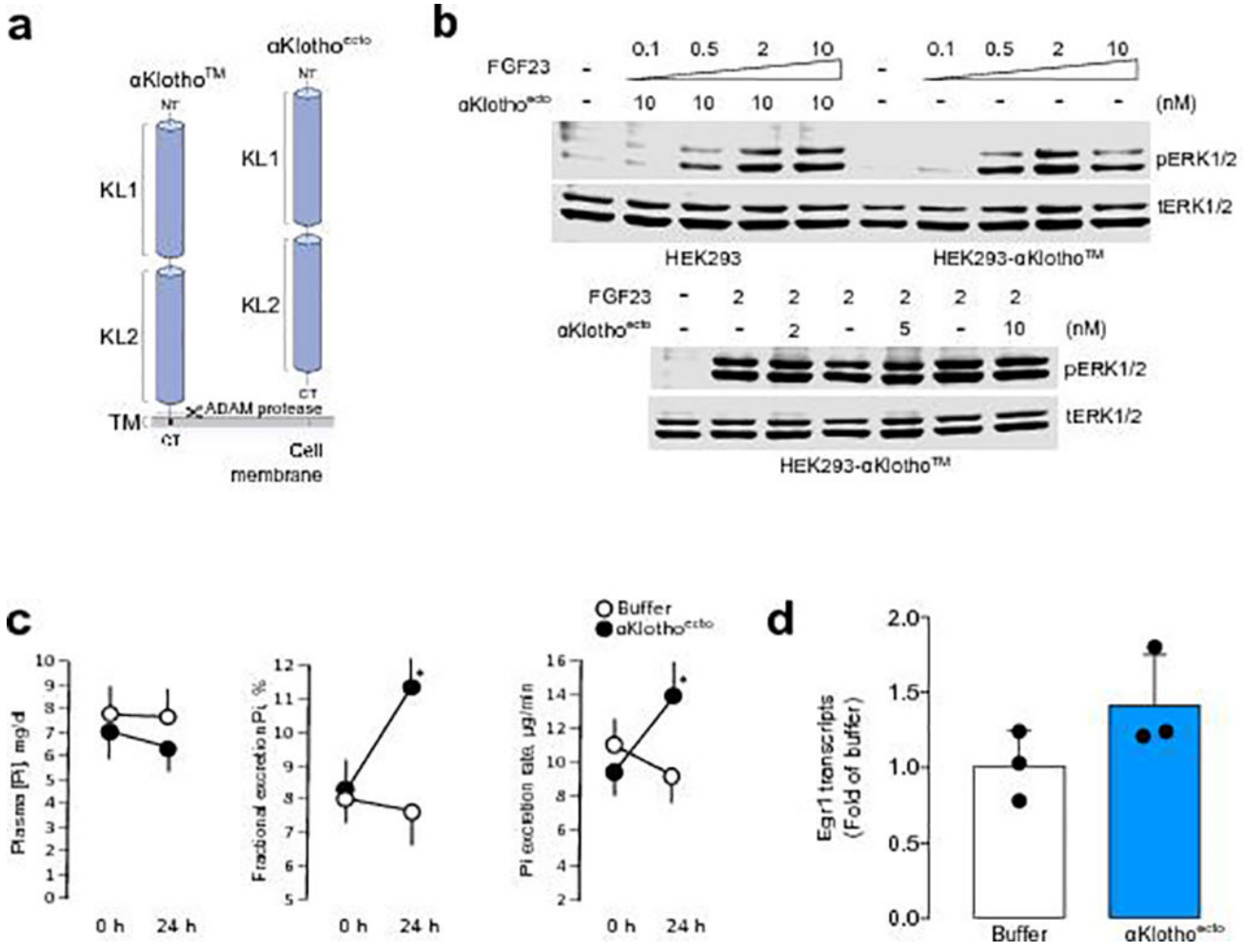

Extended Data Figure 1. αKlotho^{ecto} functions as a coreceptor for FGF23

(**a**) Domain organization of membrane-bound αKlotho (αKlotho™) and its soluble isoform αKlotho^{ecto} generated by an ectodomain shedding in the kidney[50]. KL1 and KL2: tandem domains with homology to family 1 glycosidases[51]. (**b**) Representative immunoblots of phosphorylated ERK (top blots) and total ERK (bottom blots; sample loading control) in total HEK293 cell lysates (n=3 independent experiments). Upper panel: lysates from untransfected HEK293 cells that were pre-treated with a fixed αKlotho^{ecto} concentration (10 nM) and then stimulated with increasing FGF23 concentrations, and lysates from HEK293-αKlotho™ cells treated with increasing concentrations of FGF23 alone. Lower panel: lysates from HEK293-αKlotho™ cells that were pre-treated with increasing αKlotho^{ecto} concentrations and then stimulated with a fixed FGF23 concentration. (**c**) Plasma phosphate, fractional excretion of phosphate, and phosphate excretion rate in wild-type mice before and after a single injection of αKlotho^{ecto} (0.1 mg/kg BW) or isotonic saline alone (buffer). Circles: mean values; error bars: SD; n=10 mice per group; * $p < 0.05$, paired Student's *t* test. (**d**) Relative Egr1 mRNA levels in the kidney of wild-type mice after a single injection with αKlotho^{ecto} (0.1 mg/kg BW) or isotonic saline alone (buffer). Bars: mean values; error

bars: SD; n=3 mice per group. The same batch of αKlotho^{ecto} protein was used in the experiments shown in panels (**b**) to (**d**).

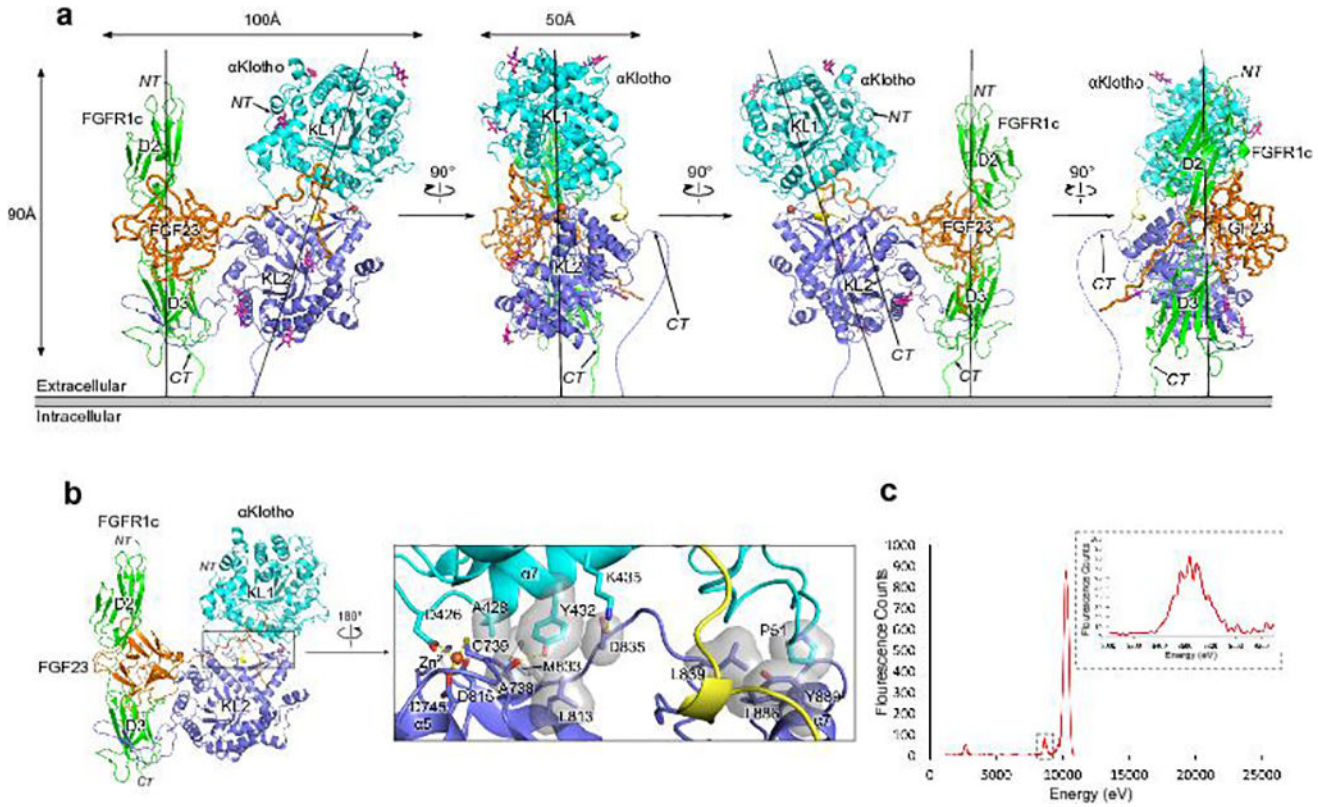

Extended Data Figure 2. Topology of ternary complex is consistent with its orientation on the cell surface

(**a**) Cartoon representation of 1:1:1 FGF23-FGFR1c^{ecto}-αKlotho^{ecto} complex in four different orientations related by 90° rotation. αKlotho domains are colored cyan (KL1) and blue (KL2); KL1-KL2 linker is in yellow. FGFR1c and FGF23 are in green and orange, respectively. The ternary complex resembles an oblique rectangular prism with an average dimension of 100 Å × 90 Å × 50 Å. The long axes of αKlotho^{ecto} and FGF23-FGFR1c complex in the ternary complex are each about 90 Å long, and parallel to one another such that the C-termini of FGFR1c^{ecto} and αKlotho^{ecto} end up on the same side of the ternary complex, ready to insert into the cell membrane (gray bar). First N-acetyl glucosamine moiety (purple sticks) at six of the seven consensus N-linked αKlotho glycosylation sites could be built due to sufficient electron density. Asn-694 is the only glycosylation site that falls in the vicinity of a binding interface, namely αKlotho^{ecto}–FGF23. (**b**) Close-up view of KL1-KL2 interdomain interface. Zinc (orange sphere)-mediated contacts facilitate overall αKlotho^{ecto} conformation. Dashed yellow lines: hydrogen bonds; gray surfaces: hydrophobic contacts. (**c**) Emission energy spectrum obtained from excitation/emission scan of FGF23-FGFR1c^{ecto}-αKlotho^{ecto} crystal. Inset: expanded view of zinc fluorescence at 8,637 eV of emission energy.

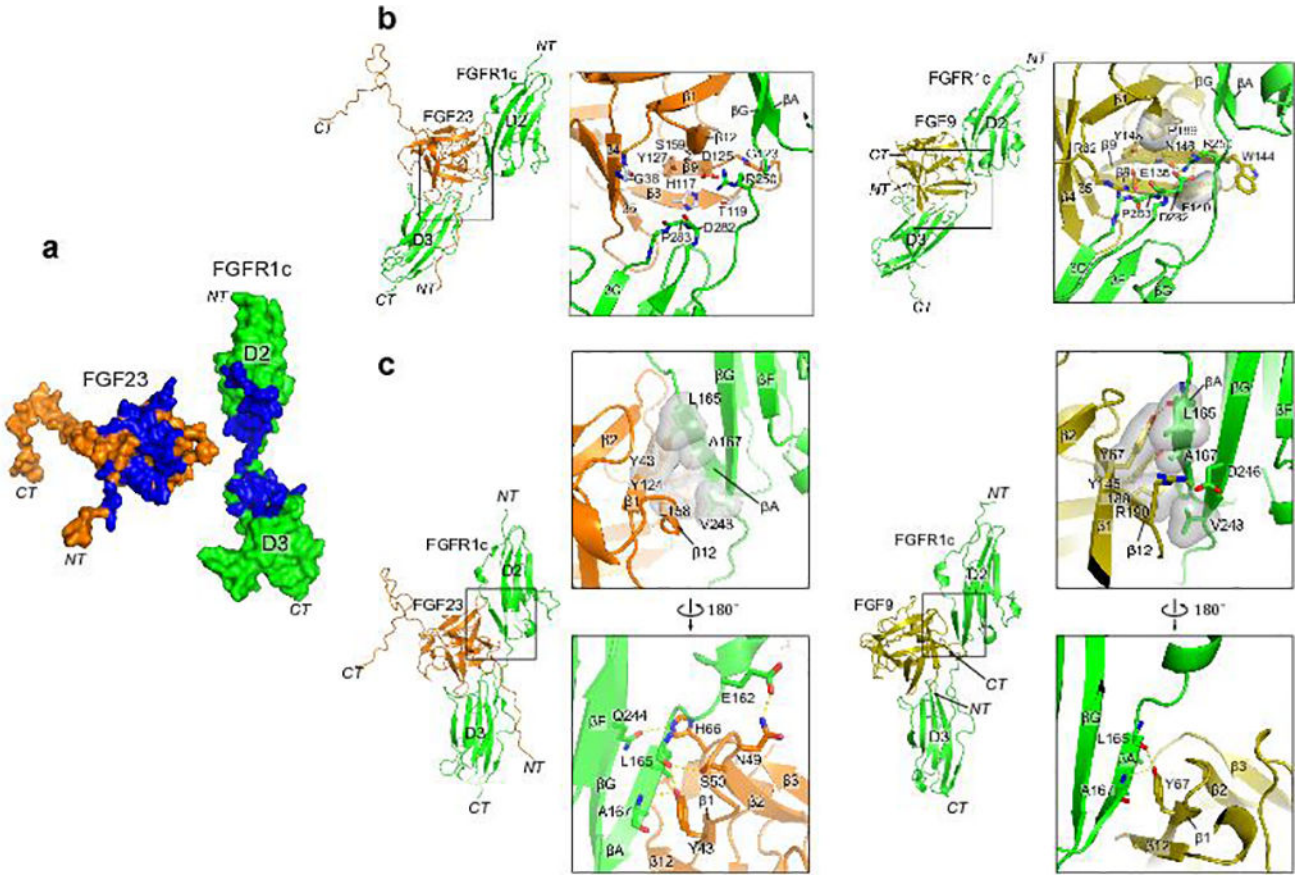

Extended Data Figure 3. Structural basis for FGF23's weak FGFR-binding affinity

(**a**) Open-book view of FGF23-FGFR1c^{ecto} complex interface. FGF23 (orange) and FGFR1c^{ecto} (green) are pulled apart and rotated by 90° around the vertical axis to expose the binding interface (blue). (**b**) Ligand–receptor D3 and ligand–receptor D2-D3 linker interfaces of endocrine FGF23-FGFR1c and paracrine FGF9-FGFR1c[52] structures. Gray transparent surfaces: hydrophobic interactions; dashed yellow lines: hydrogen bonds. Because FGF9 Arg-62 is replaced with glycine in FGF23 (Gly-38) and FGF9 Glu-138 is replaced with histidine in FGF23 (His-117), neither the side chain of Asp-125 in FGF23 (Asn-146 in FGF9), nor the side chain of invariant Arg-250 in the FGFR1c D2-D3 linker can be tethered through intramolecular hydrogen bonds. Thus, these side chains possess greater freedom of motion in the FGF23-FGFR1c complex, and as a result, hydrogen bonding between FGF23 and FGFR1c D2-D3 linker entails greater entropic cost, which generates less binding affinity. Substitution of Phe-140 and Pro-189 in FGF9 with hydrophilic Thr-119 and Ser-159 in FGF23 further diminishes the ability of FGF23 to gain binding affinity from hydrogen bonding with FGFR1c D2-D3 linker. A lack of contacts between FGF23 N-terminus and FGFR1c D3 cleft, which forms between alternatively spliced βC'-βE and βB'-βC loops[53], likely further exacerbates FGF23's weak FGFR-binding affinity. (**c**) Ligand–receptor D2 interface in endocrine FGF23-FGFR1c and paracrine FGF9-FGFR1c[52] structures. Gray transparent surfaces: hydrophobic interactions; dashed yellow lines: hydrogen bonds. Many contacts at this interface are conserved between paracrine FGFs and FGF23, and hence FGF23 gains much of its FGFR-binding affinity through these contacts.

Three hydrogen bonds involving Asn-49, Ser-50, and His-66 of FGF23 are unique to the FGF23-FGFR1c complex.

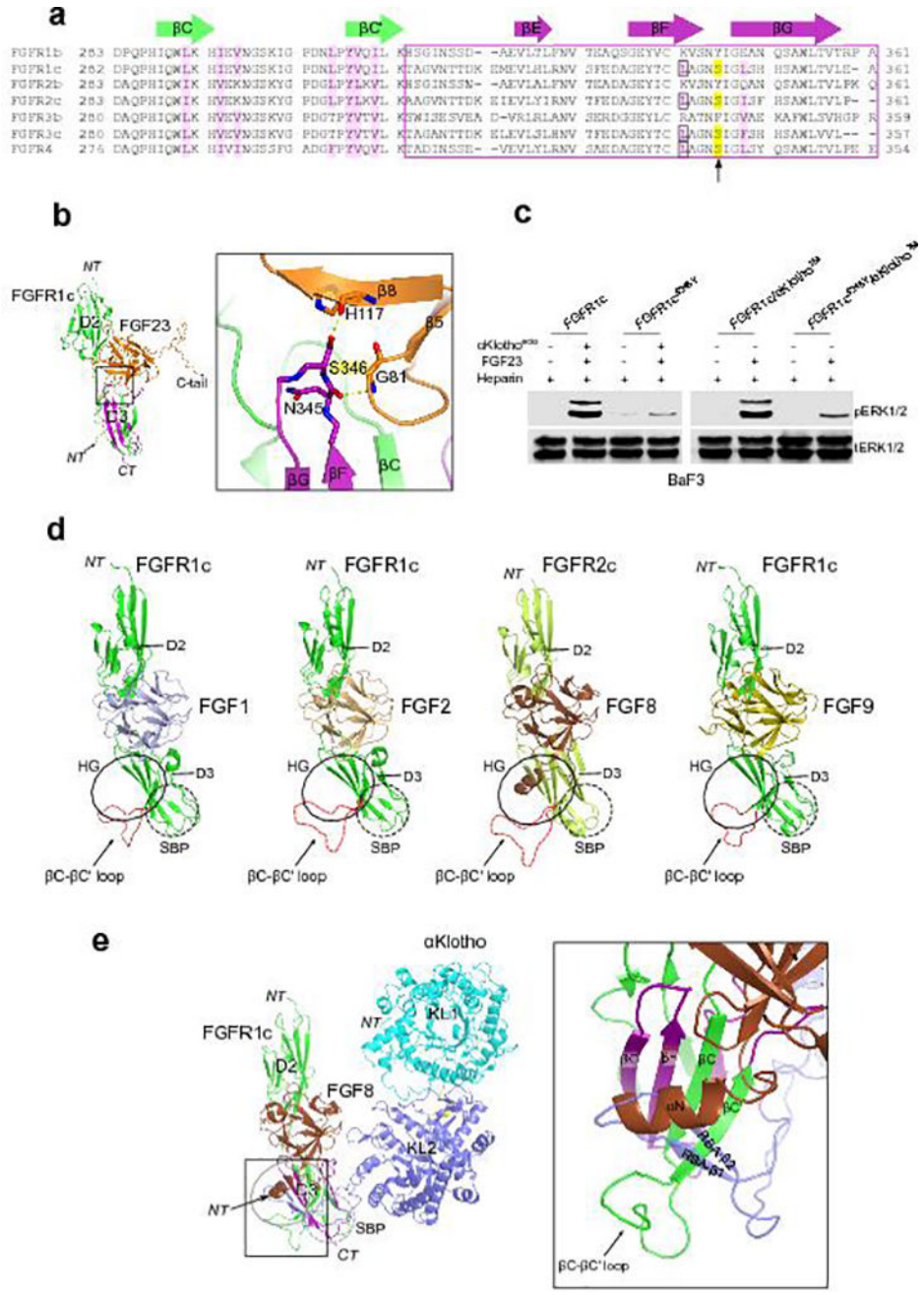

Extended Data Figure 4. Structural basis for FGFR isoform specificity of αKlotho and FGF23

(**a**) Structure-based sequence alignment of a segment of FGFR D3. The alternatively spliced regions of all seven FGFRs are boxed with a purple rectangle. β strand locations above the alignment are colored green (constant region) and purple (alternatively spliced region). A leucine (boxed) of hydrophobic groove residues (light purple) in the alternatively spliced region is conserved only among "c" isoforms of FGFR1-3 and FGFR4, which explains

αKlotho binding selectivity for these receptors. (**b**) Interface between FGF23 and βF-βG loop of FGFR1c D3 in the FGF23-FGFR1c structure of the ternary complex. Backbone atoms of His-117 and Gly-81 in FGF23 make specific hydrogen bonds with Ser-346 side-chain and Asn-345 backbone atoms of the βF-βG loop. Serine corresponding to Ser-346 in FGFR1c (yellow) is conserved only among "c" isoforms of FGFR1-3 and FGFR4 (see panel **a**). (**c**) Representative immunoblots of phosphorylated ERK (top blot) and total ERK (bottom blot; sample loading control) in total BaF3 cell lysates (n=3 independent experiments). (**d**) Cartoon representations of four paracrine FGF-FGFR complex structures[1–4]. Solid black oval: hydrophobic D3 groove. Dashed black circle: second binding pocket (SBP) for αKlotho in D3. While the hydrophobic groove is engaged by FGF8 (see also panel **e**), the SBP is not utilized in any of the current paracrine FGF-FGFR structures. In most paracrine FGF-FGFR structures, the βC-βC' loop is disordered (dashed red lines) since it does not participate in FGF binding. Evidently, SBP and βC-βC' loop in D3 have evolved to mediate αKlotho binding to FGFR. (**e**) αKlotho and FGF8b both bind to the hydrophobic groove in FGFR1c D3. FGF8b (brown) from the FGF8b-FGFR2c structure[3] was superimposed onto FGF23 in the FGF23-FGFR1c^{ecto}-αKlotho^{ecto} complex. The αN helix of FGF8b occupies the same binding pocket in FGFR1c D3 as the distal tip of αKlotho RBA.

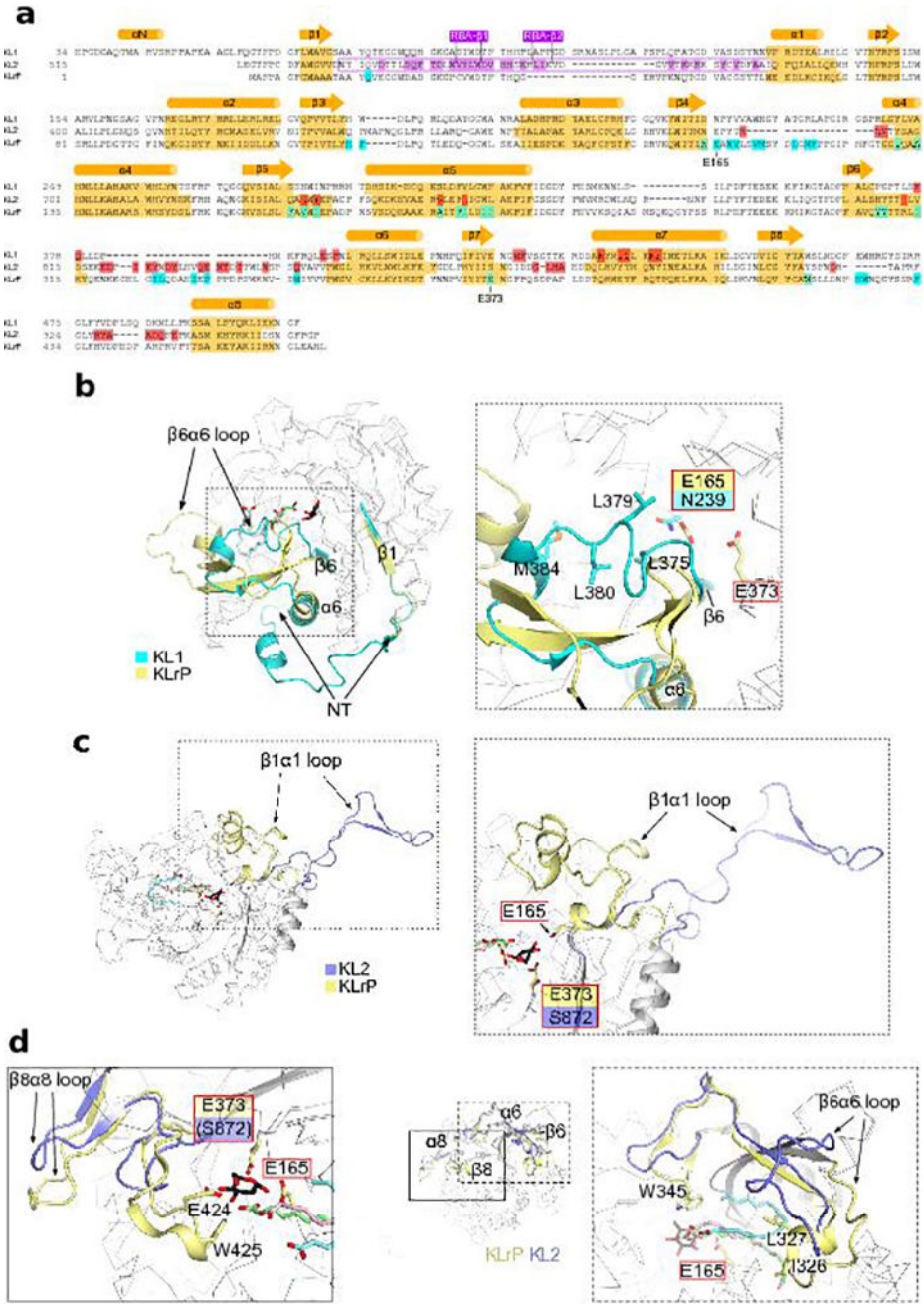

Extended Data Figure 5. αKlotho is the first non-enzymatic scaffold among TIM barrel proteins

(**a**) Structure-based sequence alignment of TIM barrels of αKlotho KL1 and KL2 domains and Klotho Related Protein (KLrP). Most glycoside hydrolases (GH), a functionally diverse group of enzymes that cleave glycosidic bonds of complex carbohydrates on glycoproteins[51], adopt TIM barrel fold. Locations and lengths of TIM barrel β-strands and α-helices are indicated above the alignment. Among GH family 1 members of the Klotho subfamily, only KLrP has a verified glycosylceramidase activity[54], and E165 and E373 are its catalytically essential glutamic acids. KLrP residues colored cyan participate in substrate recognition/hydrolysis. αKlotho residues colored red bind FGF23, and αKlotho residues of

the KL2 β1α1 loop (purple box) colored purple interact with the FGFR1c D3 domain. (**b**) Superimposition of KL1 Cα trace (gray/cyan) onto that of KLrP (gray/yellow). Superimposition RMSD is 1.08 Å. Structurally most divergent regions between KL1 and KLrP are in cartoon representation. Glucose moiety and aliphatic chains of glucosylceramide (KLrP substrate) are in sticks with carbon in black (glucose) or green/cyan/pink (aliphatic chains). Catalytically essential Glu-165 in KLrP is replaced by an asparagine in KL1. Hydrophobic residues from KL1 β6-α6 loop occupy the pocket that accommodates the aliphatic chains of glucosylceramide in KLrP. KL1 N-terminus supports KL1-KL2 cleft formation (Extended Data Fig. 2b) and KL1 β6-α6 loop conformation contributes to a key portion of the binding pocket in this cleft for the FGF23 C-terminal tail (Fig. 3c). (**c–d**) Superimposition of KL2 Cα trace (gray/blue) onto that of KLrP (gray/yellow). Superimposition RMSD is 1.37 Å. Structurally divergent β1α1 (**c**), β6α6 and β8α8 (**d**) loops of KL2 and KLrP are rendered in cartoon. β1α1 loop in KL2 is disengaged from the central TIM barrel and stretches away from it by as much as 35 Å. Catalytically essential Glu-373 in KLrP is replaced by a serine in KL2. KLrP residues from β6α6 and β8α8 loops bind glucosylceramide (KLrP substrate); for example, W345 in the β6α6 loop and E424 and W425 in the β8α8 loop. Sequence divergence (panel **a**) and altered loop conformations are incompatible with glucosylceramide coordination by KL2. β1α1, β6α6 and β8α8 loops lie at the rim of the catalytic mouth in the TIM barrel (see Fig. 2b). Divergent conformations of these three loops in KL2 result in significant widening of the central barrel cavity in KL2, which merges with the KL1-KL2 cleft to form an expansive basin that accommodates the distal portion of the FGF23 C-terminal tail.

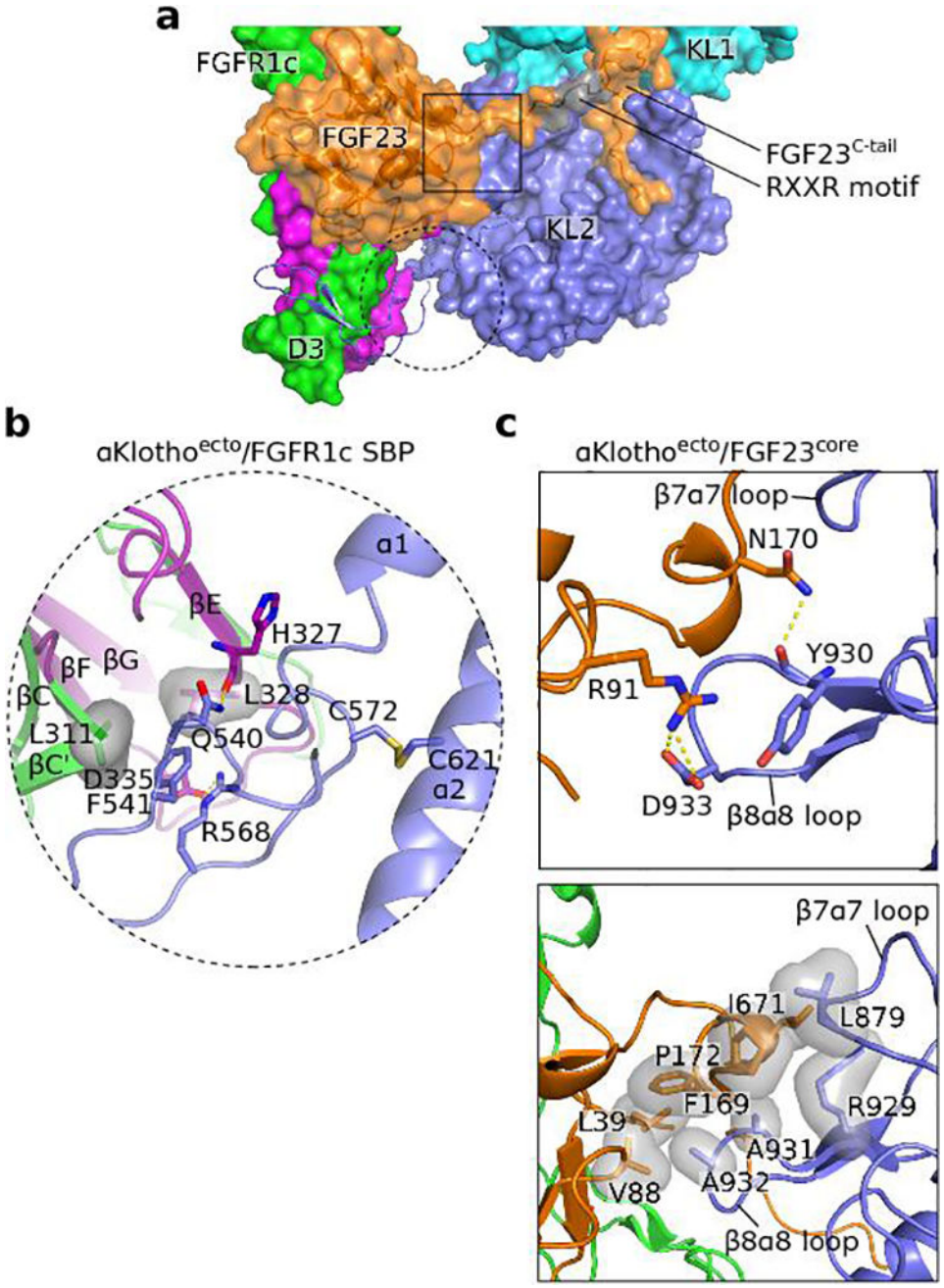

Extended Data Figure 6. αKlotho interaction with rigid core of FGF23 and a second binding pocket next to the hydrophobic groove in FGFR1c D3

(**a**) A partial view of the ternary complex. αKlotho^{ecto} (cyan/blue solid surface, receptor binding arm (RBA) of KL2 in blue cartoon), FGF23 (orange transparent surface and cartoon), FGFR1c (constant region: solid green surface; alternatively splice region: solid purple surface). Dashed black circle: perimeter of the interface between proximal end of αKlotho RBA and a second binding pocket (SBP) in FGFR1c D3 next to the hydrophobic groove. Solid black box: perimeter of αKlotho–FGF23^{core} interface. (**b**) Close-up view of the interface between proximal end of RBA and SBP in D3. Disulfide bridge between Cys-572 (N-terminal end of RBA) and Cys-621 (α2 helix) at the base of the RBA likely

imparts some degree of conformational rigidity to the proximal RBA portion, whereas the conformation of the distal RBA tip is dictated by contacts with FGFR1c D3. (**c**) Close-up view of the αKlotho–FGF23^{core} interface detailing hydrogen bonding (upper panel) and hydrophobic contacts (lower panel). Gray transparent surfaces: hydrophobic interactions; dashed yellow lines: hydrogen bonding contacts.

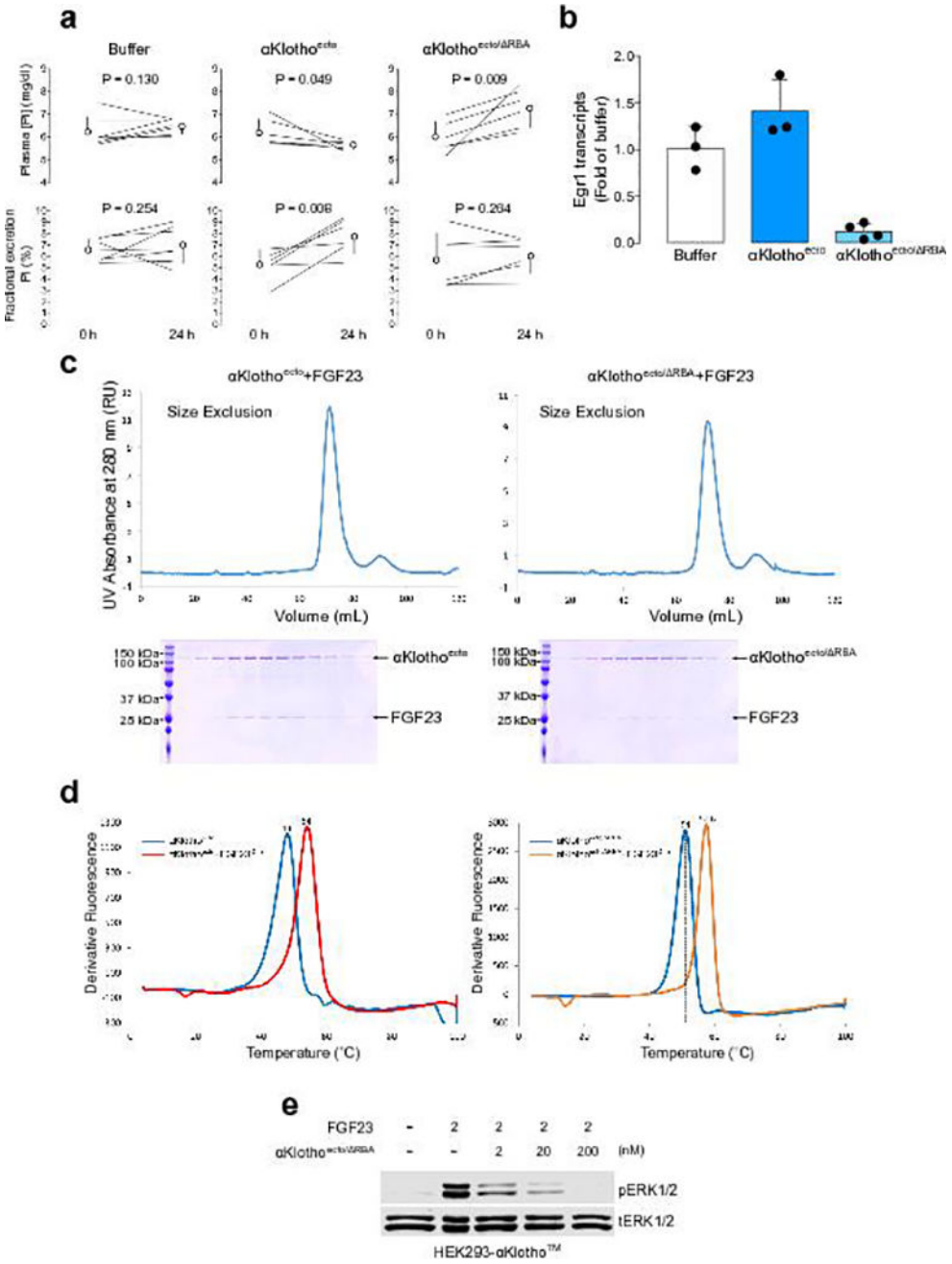

Extended Data Figure 7. Deletion of receptor binding arm of αKlotho^{ecto} generates an FGF23 ligand trap

(**a**) Plasma phosphate and fractional excretion of phosphate in wild-type mice before and after a single injection of αKlotho^{ecto} (0.1 mg/kg BW), mutant αKlotho$^{ecto/ΔRBA}$ (0.1 mg/kg

BW), or isotonic saline alone (buffer). Circles: mean values; error bars: SD; n=6 mice per group; p: significance value determined by a paired Student's *t* test. (**b**) Relative Egr1 mRNA levels in the kidney of wild-type mice injected once with αKlotho^{ecto} (0.1 mg/kg BW; n=3), mutant αKlotho$^{ecto/\Delta RBA}$ (0.1 mg/kg BW; n=4), or isotonic saline alone (buffer; n=3). Bars: mean values; error bars: SD. (**c**) Representative elution profiles of FGF23/αKlotho^{ecto} and FGF23/αKlotho$^{ecto/\Delta RBA}$ mixtures from a size-exclusion column and representative Coomassie Brilliant Blue-stained SDS-polyacrylamide gels of eluted protein peak fractions. (**d**) Thermal shift assay of αKlotho^{ecto} and αKlotho$^{ecto/\Delta RBA}$ mutant in the presence and absence of FGF23 C-terminal tail peptide (FGF23$^{C\text{-}tail}$) (n=3 independent experiments). Increased melting temperatures in the presence of the FGF23$^{C\text{-}tail}$ indicate interaction of both αKlotho^{ecto} proteins with the peptide. Higher melting temperature of αKlotho$^{ecto/\Delta RBA}$ mutant relative to wild-type αKlotho^{ecto} indicates greater stability of the mutant protein. (**e**) Representative immunoblots of phosphorylated ERK (top blot) and total ERK (bottom blot; sample loading control) in total lysates from HEK293-αKlotho™ cells co-stimulated with a fixed FGF23 concentration and increasing αKlotho$^{ecto/\Delta RBA}$ concentrations (n=3 independent experiments). αKlotho$^{ecto/\Delta RBA}$ mutant inhibits FGF23-induced ERK phosphorylation due to sequestering FGF23 into inactive FGF23-αKlotho$^{ecto/\Delta RBA}$ binary complexes. This also explains why αKlotho$^{ecto/\Delta RBA}$ injection into mice causes an increase in plasma phosphate (panel **a**) concomitant with renal Egr1 gene repression (panel **b**).

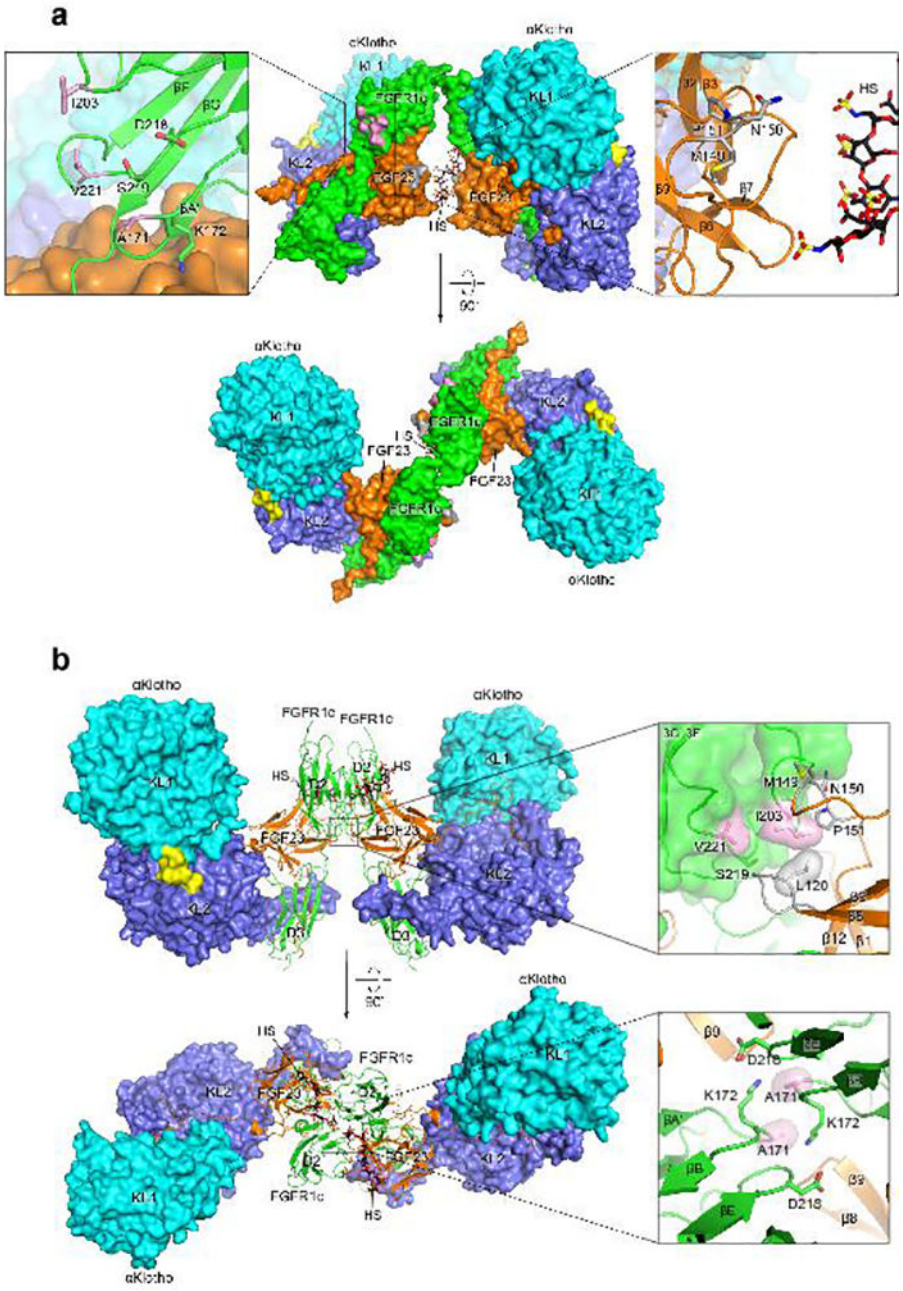

Extended Data Figure 8. FGF23-FGFR1c^{ecto}-αKlotho^{ecto}-HS quaternary dimer models

(**a**) A 2:2:2:1 FGF23-FGFR1c^{ecto}-αKlotho^{ecto}-HS quaternary dimer in two orientations related by a 90° rotation around the horizontal axis. The dimer was constructed by superimposing FGF23 from two copies of 1:1:1 FGF23-FGFR1c^{ecto}-αKlotho^{ecto} complex onto the two FGF1 molecules in the 2:2:1 FGF1-FGFR2c-HS dimer[55–58]. The dimer is held together solely by HS, which bridges two FGF23 molecules in *trans*. Boxed pink surface: location of Ala-171, Ile-203, and Val-221 of FGFR1c, the mutation of which impairs the ability of HS to induce 2:2:2:2 quaternary dimer formation (Fig. 5f). Boxed gray region: location of Met-149, Asn-150, and Pro-151 of FGF23, the mutation of which diminishes

HS-induced quaternary dimerization (Fig. 5e and 5f). None of these residues plays any role in 2:2:2:1 quaternary dimer formation, and hence, contrary to experimental evidence (Fig. 5), mutation of these residues should not impact HS-induced FGF23-FGFR1c^{ecto}-αKlotho^{ecto} dimerization. (**b**) A 2:2:2:2 FGF23-FGFR1c^{ecto}-αKlotho^{ecto}-HS quaternary dimer in two orientations related by a 90° rotation around the horizontal axis. See also Fig. 5g. The dimer was constructed by superimposing FGF23 from two copies of 1:1:1 FGF23-FGFR1c^{ecto}-αKlotho^{ecto} complex onto the two FGF2 molecules in the 2:2:2 FGF2-FGFR1c-HS dimer[59]. Insets: close-up views of the secondary FGF-FGFR (upper inset) and direct FGFR-FGFR (lower inset) interfaces. Gray/pink transparent surfaces: hydrophobic interactions. Mutation of Ala-171, Ile-203, and Val-221 (pink) impairs the ability of HS to dimerize FGF23-FGFR1c^{ecto}-αKlotho^{ecto} ternary complex (Fig. 5f).

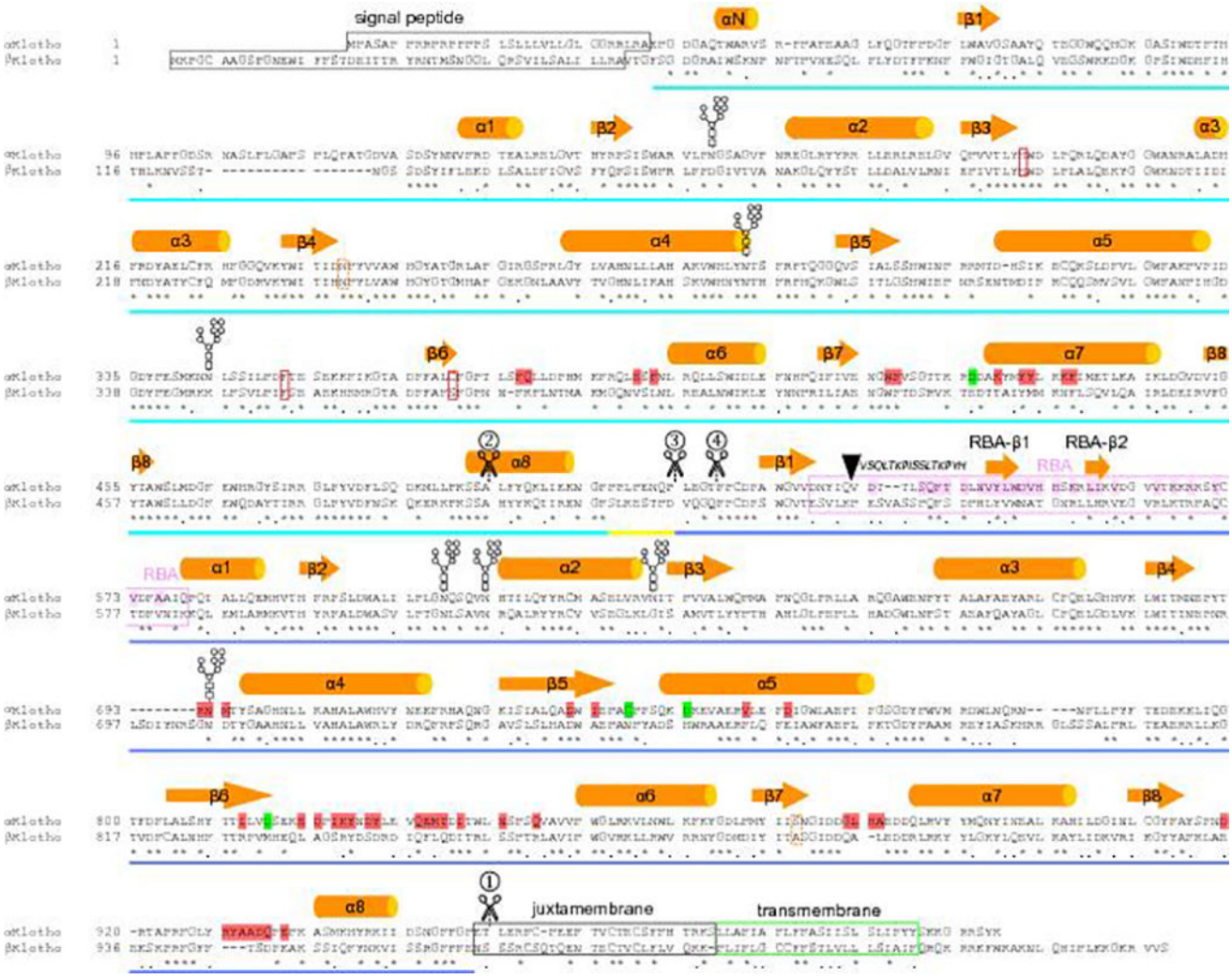

Extended Data Figure 9. FGF19/FGF21 co-receptor βKlotho is a non-enzymatic scaffold protein analogous to αKlotho

Structure-based sequence alignment of αKlotho and βKlotho. The locations of the eight alternating β-strands and α-helices of the TIM fold are indicated above the alignment. Cyan, blue, and yellow bars below the alignment mark the domain boundaries of KL1, KL2, and

KL1-KL2 linker. Asterisks denote sequence identity and dots denote sequence similarity. Scissor symbols mark the four proposed sites of αKlotho cleavage by ADAM proteases/secretases. Cleavage 1, which coincides with the end of the rigid core of KL2, results in shedding of the entire αKlotho ectodomain from the cell membrane. While this cleavage product is a functional co-receptor, the αKlotho fragments generated by cleavages 2, 3, and 4 would be devoid of co-receptor activity. Black triangle: site where alternative splicing replaces the C-terminal KL2 sequence with a 15-residue-long unrelated sequence. Glycan chain symbols: seven predicted N-linked glycosylation sites. Zn^{2+}-chelating residues of αKlotho are green, FGFR1c-binding residues are light purple, and FGF23-binding residues are red. Light purple box: β1α1 loop sequence in KL2 termed RBA. βKlotho RBA is about as long as αKlotho RBA, and key FGFR-binding residues are conserved between these two RBAs, which is consistent with the similar FGFR-binding specificity of αKlotho and βKlotho[60,61]. But αKlotho residues in the binding pockets for the FGF23 C-terminal tail are not conserved in βKlotho, conforming to major sequence differences between the C-terminal tails of FGF23 and FGF19/FGF21 (Extended Data Fig. 10a).

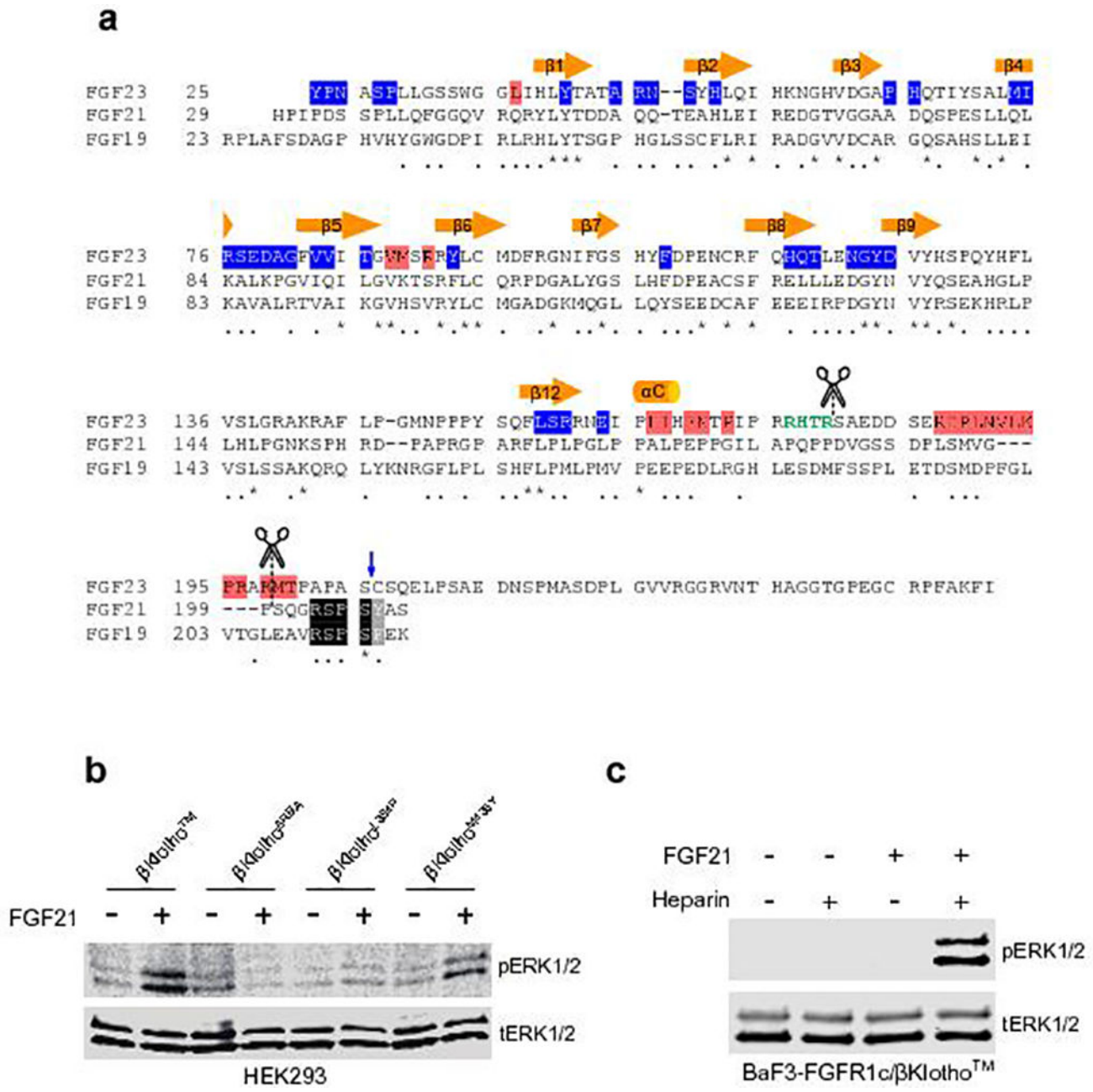

Extended Data Figure 10. βKlotho-dependent FGFR activation by FGF19/FGF21 is mechanistically similar to αKlotho-dependent FGFR activation by FGF23

(**a**) Structure-based sequence alignment of endocrine FGFs. β-strands and αC helix comprising the atypical β-trefoil core of FGF23 are indicated above the alignment. Asterisks and dots below the alignment denote sequence identity and similarity, respectively. Scissor symbols mark inactivating proteolytic cleavage sites in FGF23 and FGF21[62]. RXXR cleavage motif in FGF23 is in green bold letters. FGFR1c-binding residues of FGF23 are colored blue, αKlotho-binding residues are colored red. Vertical blue arrow marks the C-terminal boundary of the FGF23 variant used to solve the FGF23-FGFR1c^{ecto}-αKlotho^{ecto} complex structure. Five residues at the distal C-terminal region of FGF19/FGF21 (black/

gray) mediate binding of FGF19/FGF21 to βKlotho. These residues completely diverge from the αKlotho-binding residues in the FGF23 C-terminal tail. αKlotho-binding residues in the FGF23 core also are not conserved in FGF19/FGF21. (**b**) Representative immunoblots of phosphorylated ERK (top blot) and total ERK (bottom blot; sample loading control) in total lysates from HEK293 cells expressing wild-type or mutant βKlotho™ (n=3 independent experiments). Similar to αKlotho$^{\Delta RBA}$, βKlotho$^{\Delta RBA}$ failed to support FGF21-induced FGFR activation, and βKlotho^{L394P} and βKlotho^{M435Y} mutants also had greatly diminished ability to promote FGF21 signaling. Thus, βKlotho tethers FGFR1c and FGF21 to itself in a manner similar to that identified for αKlotho to enable FGF21 signaling. (**c**) Representative immunoblots of phosphorylated ERK (top blot) and total ERK (bottom blot; sample loading control) in total lysates from BaF3 cells expressing FGFR1c and βKlotho™ (n=3 independent experiments). Like αKlotho, βKlotho also requires heparin to support FGF21-mediated FGFR1c activation.

Extended Data Table 1

X-ray Data Collection, Structure Refinement Statistics Values in parenthesis are for the highest resolution shell.

Protein	**FGF23-FGFR1c^{ecto}-αKlotho^{ecto}**
Data Collection	
X-ray wavelength (Å)	0.97918
Space group	C2
Unit Cell Dimensions	
a, b, c (Å)	283.31, 72.60, 95.33
α, β, γ (°)	90.00, 91.98, 90.00
Resolution (Å)	50–3.00 (3.18–3.0)
No. measured reflections	294862
No. unique reflections	39077
Data redundancy	7.5 (7.6)
Data completeness (%)	99.7 (98.8)
R_{meas} (%)	20.7 (138.0)
Signal (<I/σI>)	11.1 (1.7)
Refinement	
Resolution (Å)	48.81–3.00 (3.08–3.00)
No. unique reflections	39042 (2766)
No. reflections (R_{free})	1954 (137)
R_{work}/R_{free}	23.72 (45.41)/29.68 (53.68)
No. TLS groups	3 (one per polypeptide chain)
Number of atoms	
Protein	10466
Sugar (NAG)	98

Protein	FGF23-FGFR1c^{ecto}-αKlotho^{ecto}
Glutathione (GSH)	40
Ion (Zn^{2+})	1
Solvent	1
R.m.s. deviations	
Bond length (Å)	0.002
Bond angle (°)	0.498
Average B factors (Å^2)	
Protein	114
Sugar (NAG)	180
Glutathione (GSH)	170
Ion (Zn^{2+})	116
Solvent	58
Ramachandran Plot	
Favored (%)	89.39
Allowed (%)	9.60
Outliers (%)	1.01
Rotamer outliers (%)	0
No. Cβ Deviations	0
All-Atom Clashscore	7.7
PDB ID	5W21

Supplementary Material

Refer to Web version on PubMed Central for supplementary material.

Acknowledgments

We thank Dr. Nicholas J. Cowan for critically reading and editing the manuscript, and Dr. Ching-Shin Huang for help with diffraction data processing with XDS. This work was primarily supported by NIH grant R01 DE13686 (to M.M.). Support was also provided by National Key R&D Program of China (#2017YFA0506000 to X.L.). Funding for mouse studies was provided by R01 DK092461, P30 DK079328 (to O.W.M.), and R01 DK091392 (to M.C.H). Beamlines at the Northeastern Collaborative Access Team (NE-CAT) facility at the Advanced Photon Source of Argonne National Laboratory are primarily funded by NIH NIGMS and member institutions.

References

1. Shimada T, et al. Targeted ablation of Fgf23 demonstrates an essential physiological role of FGF23 in phosphate and vitamin D metabolism. J Clin Invest. 2004; 113:561–568. DOI: 10.1172/JCI19081 [PubMed: 14966565]
2. Gattineni J, et al. FGF23 decreases renal NaPi-2a and NaPi-2c expression and induces hypophosphatemia in vivo predominantly via FGF receptor 1. Am J Physiol Renal Physiol. 2009; 297:F282–291. DOI: 10.1152/ajprenal.90742.2008 [PubMed: 19515808]

3. Lemmon MA, Schlessinger J. Cell signaling by receptor tyrosine kinases. Cell. 2010; 141:1117–1134. DOI: 10.1016/j.cell.2010.06.011 [PubMed: 20602996]
4. Schlessinger J, et al. Crystal structure of a ternary FGF-FGFR-heparin complex reveals a dual role for heparin in FGFR binding and dimerization. Mol Cell. 2000; 6:743–750. [PubMed: 11030354]
5. Mohammadi M, Olsen SK, Ibrahimi OA. Structural basis for fibroblast growth factor receptor activation. Cytokine Growth Factor Rev. 2005; 16:107–137. DOI: 10.1016/j.cytogfr.2005.01.008 [PubMed: 15863029]
6. Goetz R, Mohammadi M. Exploring mechanisms of FGF signalling through the lens of structural biology. Nat Rev Mol Cell Biol. 2013; 14:166–180. DOI: 10.1038/nrm3528 [PubMed: 23403721]
7. Kuro-o M, et al. Mutation of the mouse klotho gene leads to a syndrome resembling ageing. Nature. 1997; 390:45–51. DOI: 10.1038/36285 [PubMed: 9363890]
8. Henrissat B, Davies G. Structural and sequence-based classification of glycoside hydrolases. Curr Opin Struct Biol. 1997; 7:637–644. [PubMed: 9345621]
9. Goetz R, et al. Molecular insights into the klotho-dependent, endocrine mode of action of fibroblast growth factor 19 subfamily members. Mol Cell Biol. 2007; 27:3417–3428. DOI: 10.1128/MCB.02249-06 [PubMed: 17339340]
10. Goetz R, et al. Isolated C-terminal tail of FGF23 alleviates hypophosphatemia by inhibiting FGF23-FGFR-Klotho complex formation. Proc Natl Acad Sci U S A. 2010; 107:407–412. DOI: 10.1073/pnas.0902006107 [PubMed: 19966287]
11. Urakawa I, et al. Klotho converts canonical FGF receptor into a specific receptor for FGF23. Nature. 2006; 444:770–774. DOI: 10.1038/nature05315 [PubMed: 17086194]
12. Kurosu H, et al. Regulation of fibroblast growth factor-23 signaling by klotho. J Biol Chem. 2006; 281:6120–6123. DOI: 10.1074/jbc.C500457200 [PubMed: 16436388]
13. Li SA, et al. Immunohistochemical localization of Klotho protein in brain, kidney, and reproductive organs of mice. Cell Struct Funct. 2004; 29:91–99. [PubMed: 15665504]
14. van Loon EP, et al. Shedding of klotho by ADAMs in the kidney. Am J Physiol Renal Physiol. 2015; 309:F359–368. DOI: 10.1152/ajprenal.00240.2014 [PubMed: 26155844]
15. Lindberg K, et al. The kidney is the principal organ mediating klotho effects. J Am Soc Nephrol. 2014; 25:2169–2175. DOI: 10.1681/ASN.2013111209 [PubMed: 24854271]
16. Chen CD, Podvin S, Gillespie E, Leeman SE, Abraham CR. Insulin stimulates the cleavage and release of the extracellular domain of Klotho by ADAM10 and ADAM17. Proc Natl Acad Sci U S A. 2007; 104:19796–19801. DOI: 10.1073/pnas.0709805104 [PubMed: 18056631]
17. Imura A, et al. Secreted Klotho protein in sera and CSF: implication for post-translational cleavage in release of Klotho protein from cell membrane. FEBS Lett. 2004; 565:143–147. DOI: 10.1016/j.febslet.2004.03.090 [PubMed: 15135068]
18. Matsumura Y, et al. Identification of the human klotho gene and its two transcripts encoding membrane and secreted klotho protein. Biochem Biophys Res Commun. 1998; 242:626–630. [PubMed: 9464267]
19. Shiraki-Iida T, et al. Structure of the mouse klotho gene and its two transcripts encoding membrane and secreted protein. FEBS Lett. 1998; 424:6–10. [PubMed: 9537505]
20. Kurosu H, et al. Suppression of aging in mice by the hormone Klotho. Science. 2005; 309:1829–1833. DOI: 10.1126/science.1112766 [PubMed: 16123266]
21. Hu MC, Shiizaki K, Kuro-o M, Moe OW. Fibroblast growth factor 23 and Klotho: physiology and pathophysiology of an endocrine network of mineral metabolism. Annu Rev Physiol. 2013; 75:503–533. DOI: 10.1146/annurev-physiol-030212-183727 [PubMed: 23398153]
22. Chang Q, et al. The beta-glucuronidase klotho hydrolyzes and activates the TRPV5 channel. Science. 2005; 310:490–493. DOI: 10.1126/science.1114245 [PubMed: 16239475]
23. Cha SK, et al. Removal of sialic acid involving Klotho causes cell-surface retention of TRPV5 channel via binding to galectin-1. Proc Natl Acad Sci U S A. 2008; 105:9805–9810. DOI: 10.1073/pnas.0803223105 [PubMed: 18606998]
24. Hu MC, et al. Klotho: a novel phosphaturic substance acting as an autocrine enzyme in the renal proximal tubule. Faseb Journal. 2010; 24:3438–3450. DOI: 10.1096/fj.10-154765 [PubMed: 20466874]

25. Imura A, et al. alpha-Klotho as a regulator of calcium homeostasis. Science. 2007; 316:1615–1618. DOI: 10.1126/science.1135901 [PubMed: 17569864]
26. Hayashi Y, et al. Klotho-related protein is a novel cytosolic neutral beta-glycosylceramidase. J Biol Chem. 2007; 282:30889–30900. DOI: 10.1074/jbc.M700832200 [PubMed: 17595169]
27. Goetz R, et al. Klotho coreceptors inhibit signaling by paracrine fibroblast growth factor 8 subfamily ligands. Mol Cell Biol. 2012; 32:1944–1954. DOI: 10.1128/MCB.06603-11 [PubMed: 22451487]
28. Andrukhova O, et al. Klotho Lacks an FGF23-Independent Role in Mineral Homeostasis. J Bone Miner Res. 2017; 32:2049–2061. DOI: 10.1002/jbmr.3195 [PubMed: 28600880]
29. Wu X, et al. C-terminal tail of FGF19 determines its specificity toward Klotho co-receptors. J Biol Chem. 2008; 283:33304–33309. DOI: 10.1074/jbc.M803319200 [PubMed: 18829467]
30. Ornitz DM, et al. Heparin is required for cell-free binding of basic fibroblast growth factor to a soluble receptor and for mitogenesis in whole cells. Mol Cell Biol. 1992; 12:240–247. [PubMed: 1309590]
31. Pellegrini L, Burke DF, von Delft F, Mulloy B, Blundell TL. Crystal structure of fibroblast growth factor receptor ectodomain bound to ligand and heparin. Nature. 2000; 407:1029–1034. DOI: 10.1038/35039551 [PubMed: 11069186]
32. Harmer NJ, et al. Towards a resolution of the stoichiometry of the fibroblast growth factor (FGF)-FGF receptor-heparin complex. J Mol Biol. 2004; 339:821–834. DOI: 10.1016/j.jmb.2004.04.031 [PubMed: 15165853]
33. Ogawa Y, et al. BetaKlotho is required for metabolic activity of fibroblast growth factor 21. Proc Natl Acad Sci U S A. 2007; 104:7432–7437. DOI: 10.1073/pnas.0701600104 [PubMed: 17452648]
34. Kurosu H, et al. Tissue-specific expression of betaKlotho and fibroblast growth factor (FGF) receptor isoforms determines metabolic activity of FGF19 and FGF21. J Biol Chem. 2007; 282:26687–26695. DOI: 10.1074/jbc.M704165200 [PubMed: 17623664]
35. Holt JA, et al. Definition of a novel growth factor-dependent signal cascade for the suppression of bile acid biosynthesis. Genes Dev. 2003; 17:1581–1591. DOI: 10.1101/gad.1083503 [PubMed: 12815072]
36. Potthoff MJ, et al. FGF21 induces PGC-1alpha and regulates carbohydrate and fatty acid metabolism during the adaptive starvation response. Proc Natl Acad Sci U S A. 2009; 106:10853–10858. DOI: 10.1073/pnas.0904187106 [PubMed: 19541642]
37. Pitteloud N, et al. Digenic mutations account for variable phenotypes in idiopathic hypogonadotropic hypogonadism. J Clin Invest. 2007; 117:457–463. DOI: 10.1172/JCI29884 [PubMed: 17235395]
50. Chen CD, Podvin S, Gillespie E, Leeman SE, Abraham CR. Insulin stimulates the cleavage and release of the extracellular domain of Klotho by ADAM10 and ADAM17. Proc Natl Acad Sci U S A. 2007; 104:19796–19801. DOI: 10.1073/pnas.0709805104 [PubMed: 18056631]
51. Henrissat B, Davies G. Structural and sequence-based classification of glycoside hydrolases. Curr Opin Struct Biol. 1997; 7:637–644. [PubMed: 9345621]
52. Liu Y, et al. Regulation of Receptor Binding Specificity of FGF9 by an Autoinhibitory Homodimerization. Structure. 2017; 25:1325–1336. e1323. DOI: 10.1016/j.str.2017.06.016 [PubMed: 28757146]
53. Belov AA, Mohammadi M. Molecular mechanisms of fibroblast growth factor signaling in physiology and pathology. Cold Spring Harb Perspect Biol. 2013; 5
54. Hayashi Y, et al. Klotho-related protein is a novel cytosolic neutral beta-glycosylceramidase. J Biol Chem. 2007; 282:30889–30900. DOI: 10.1074/jbc.M700832200 [PubMed: 17595169]
55. Pellegrini L, Burke DF, von Delft F, Mulloy B, Blundell TL. Crystal structure of fibroblast growth factor receptor ectodomain bound to ligand and heparin. Nature. 2000; 407:1029–1034. DOI: 10.1038/35039551 [PubMed: 11069186]
56. Harmer NJ, et al. Towards a resolution of the stoichiometry of the fibroblast growth factor (FGF)-FGF receptor-heparin complex. J Mol Biol. 2004; 339:821–834. DOI: 10.1016/j.jmb.2004.04.031 [PubMed: 15165853]

57. Robinson CJ, Harmer NJ, Goodger SJ, Blundell TL, Gallagher JT. Cooperative dimerization of fibroblast growth factor 1 (FGF1) upon a single heparin saccharide may drive the formation of 2:2:1 FGF1.FGFR2c.heparin ternary complexes. J Biol Chem. 2005; 280:42274–42282. DOI: 10.1074/jbc.M505720200 [PubMed: 16219767]

58. Goodger SJ, et al. Evidence that heparin saccharides promote FGF2 mitogenesis through two distinct mechanisms. J Biol Chem. 2008; 283:13001–13008. DOI: 10.1074/jbc.M704531200 [PubMed: 18281281]

59. Schlessinger J, et al. Crystal structure of a ternary FGF-FGFR-heparin complex reveals a dual role for heparin in FGFR binding and dimerization. Mol Cell. 2000; 6:743–750. [PubMed: 11030354]

60. Urakawa I, et al. Klotho converts canonical FGF receptor into a specific receptor for FGF23. Nature. 2006; 444:770–774. DOI: 10.1038/nature05315 [PubMed: 17086194]

61. Kurosu H, et al. Regulation of fibroblast growth factor-23 signaling by klotho. J Biol Chem. 2006; 281:6120–6123. DOI: 10.1074/jbc.C500457200 [PubMed: 16436388]

62. Dunshee DR, et al. Fibroblast Activation Protein Cleaves and Inactivates Fibroblast Growth Factor 21. J Biol Chem. 2016; 291:5986–5996. DOI: 10.1074/jbc.M115.710582 [PubMed: 26797127]

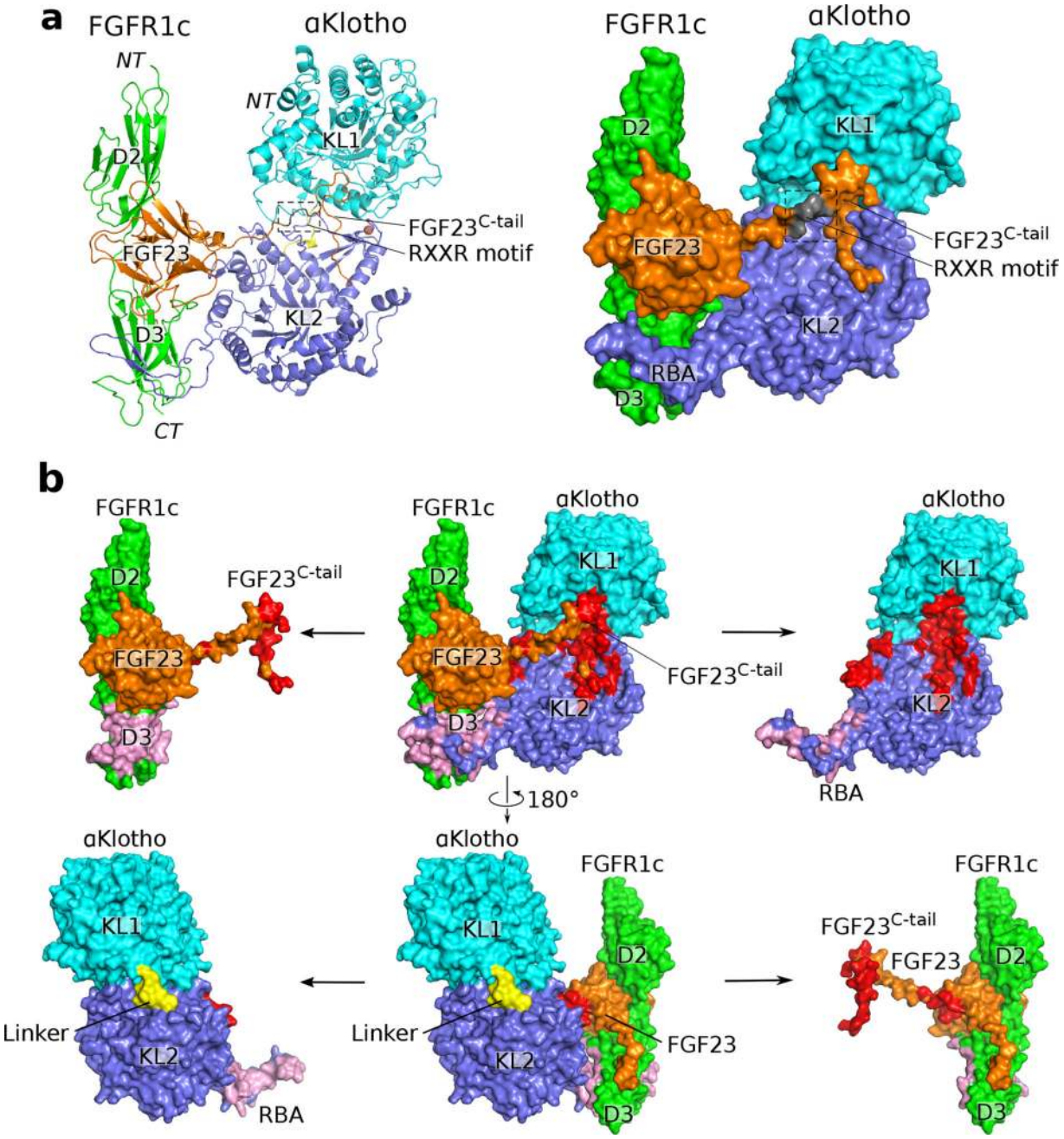

Figure 1.

Overall topology of the FGF23-FGFR1c^{ecto}-αKlotho^{ecto} complex. (**a**) Cartoon (left) and surface representation (right) of the ternary complex structure. αKlotho KL1 (cyan) and KL2 (blue) domains are joined by a short proline-rich linker (yellow; not visible in the surface presentation). FGF23 is in orange with its proteolytic cleavage motif in gray. FGFR1c is in green. NT, N-terminus; CT, C-terminus. (**b**) Binding interfaces between αKlotho^{ecto} and the FGF23-FGFR1c^{ecto} complex. The ternary complex (center) is shown in two different orientations related by a 180° rotation along the vertical axis. FGF23-αKlotho^{ecto} (red) and FGFR1c^{ecto}-αKlotho^{ecto} (pink) interfaces are visualized by pulling

αKlotho^{ecto} and FGF23-FGFR1c^{ecto} complex away from each other. The separated components are shown to the left and right of the ternary complex.

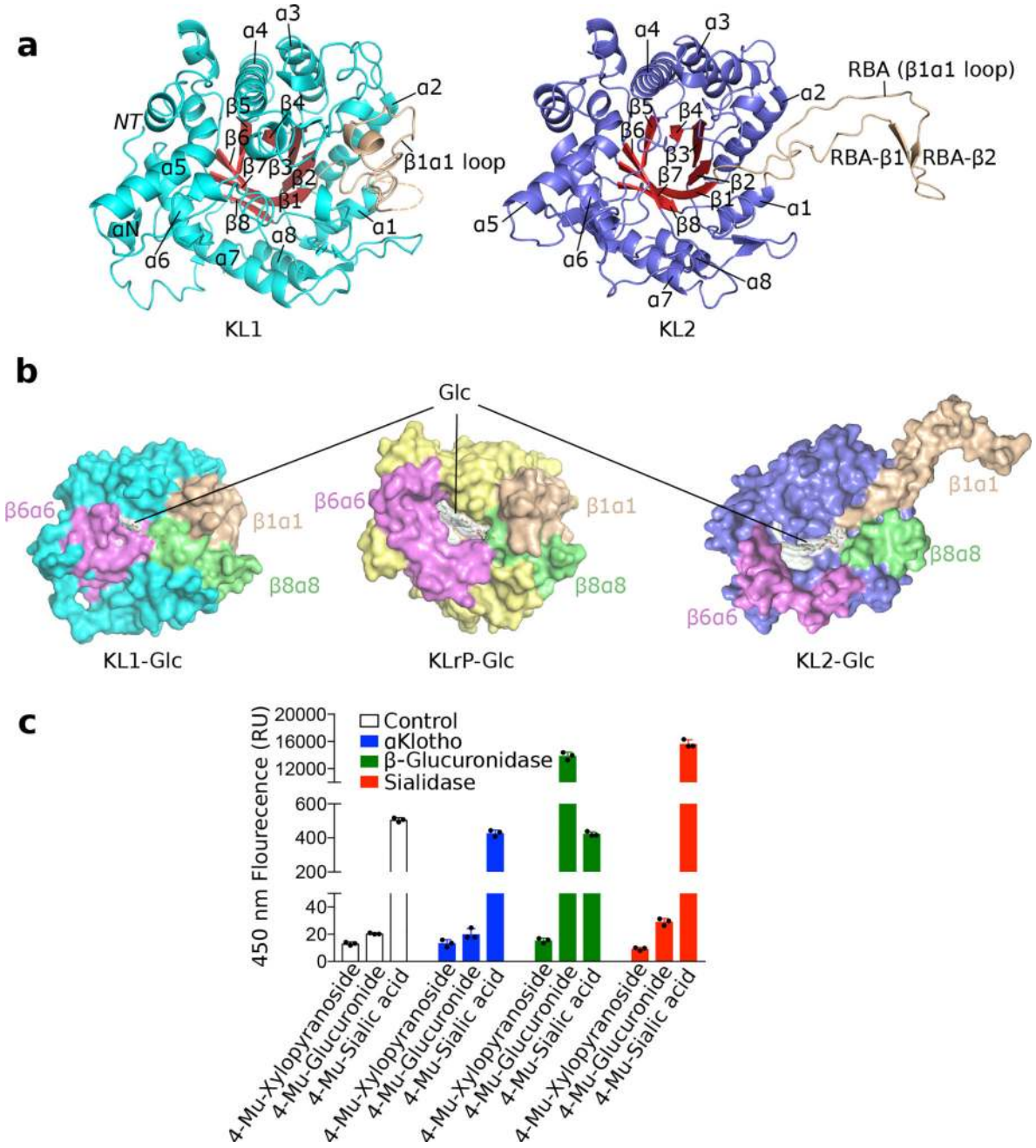

Figure 2.

αKlotho is a non-enzymatic molecular scaffold. (**a**) Triosephosphate isomerase (TIM) barrel topology of αKlotho KL1 and KL2 domains. KL1 is in the same orientation as in Fig. 1a, whereas KL2 has been superimposed onto KL1 and has thus been reoriented. The eight alternating β strands (red) and α helices (cyan/blue) which define the TIM barrel are labeled according to the standard nomenclature for the TIM fold[8]. KL1 and KL2 differ dramatically in the conformation of the β1α1 loop (wheat). In KL2, this loop protrudes away from the TIM barrel and serves as a Receptor Binding Arm (RBA; Fig. 1). (**b**) Molecular surfaces of KLrP-glucosylceramide (Glc) (center; KLrP in yellow), KL1-Glc (left; KL1 in cyan) and

KL2-Glc (right; KL2 in blue). Binding of Glc to KL1 and KL2 was simulated by superimposing KL1 and KL2 onto KLrP-Glc. In all cases, Glc is shown as pale gray sticks/surface. The divergent conformation of the β6α6 loop (pink) in KL1 almost seals off the entrance to the catalytic pocket, while the divergent conformations of β1α1 (RBA; wheat), β6α6 (pink) and β8α8 (green) loops in KL2 leave the central barrel cavity in KL2 in a more solvent-exposed state that is less capable of ligating substrate (see also Extended Data Fig. 5). (**c**) Glycosidase activity of αKlotho^{ecto}, sialidase, and β-glucuronidase. Bars: mean values; error bars: SD; dots: individual data points; n=3 independent experiments. RU, relative units.

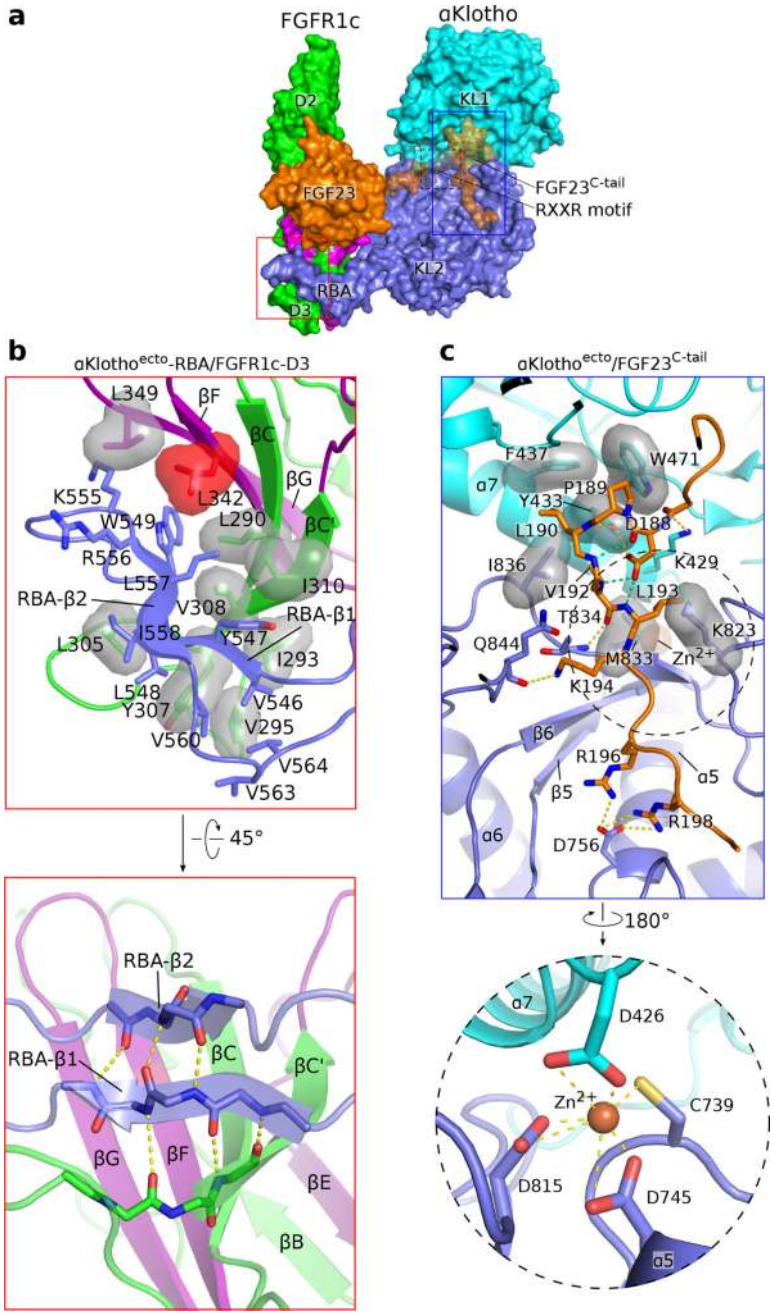

Figure 3.

αKlotho simultaneously tethers FGFR1c by its D3 domain and FGF23 by its C-terminal tail. (**a**) Ternary complex structure in surface representation. Coloring is the same as in Fig. 1a, except that the alternatively spliced region of FGFR1c is highlighted in purple. Red box: perimeter of interface between distal tip of αKlotho Receptor Binding Arm (RBA) and the hydrophobic FGFR1c D3 groove. Blue box: perimeter of αKlotho–FGF23$^{C\text{-}tail}$ interface. (**b**) RBA stretches out of the KL2 domain of αKlotho^{ecto} and latches onto the FGFR1c D3 domain. Upper panel: interface between the distal tip of RBA and the D3 groove detailing hydrophobic interactions (gray transparent surfaces). Note that Leu342 (red) from the

spliced region of the D3 groove is strictly conserved in “c” splice isoforms of FGFR1-3 and FGFR4 and is mutated in Kallmann syndrome[37]. Lower panel: Close-up view of the extended β sheet between the RBA-β1:RBA-β2 strand pair and the four-stranded β sheet in D3 (βC’-βC-βF-βG). This structure forms via hydrogen bonding (dashed yellow lines) between backbone atoms of RBA-β1 and D3-βC’. (**c**) Both KL domains of αKlotho^{ecto} participate in tethering of the flexible C-terminal tail of FGF23 (FGF23$^{C\text{-}tail}$). FGF23$^{C\text{-}tail}$ residues Asp-188 – Thr-200 thread through the KL1-KL2 cleft and the β-barrel cavity of KL2. Of these residues, Asp188 – Leu-193 adopt a cage-like conformation that is partially stabilized by intramolecular hydrogen bonds (dashed green lines). Dashed yellow lines: intermolecular hydrogen bonds; gray transparent surfaces: hydrophobic interactions. Note that Tyr-433 from the KL1 α7 helix deep inside the KL1-KL2 cleft plays a prominent role in tethering the cage-like structure in the FGF23$^{C\text{-}tail}$ formed by Asp-188 – Leu-193. Dashed circle (shown at greater magnification below): the KL1–KL2 interface where residues from both αKlotho domains jointly coordinate a Zn^{2+} ion (orange sphere).

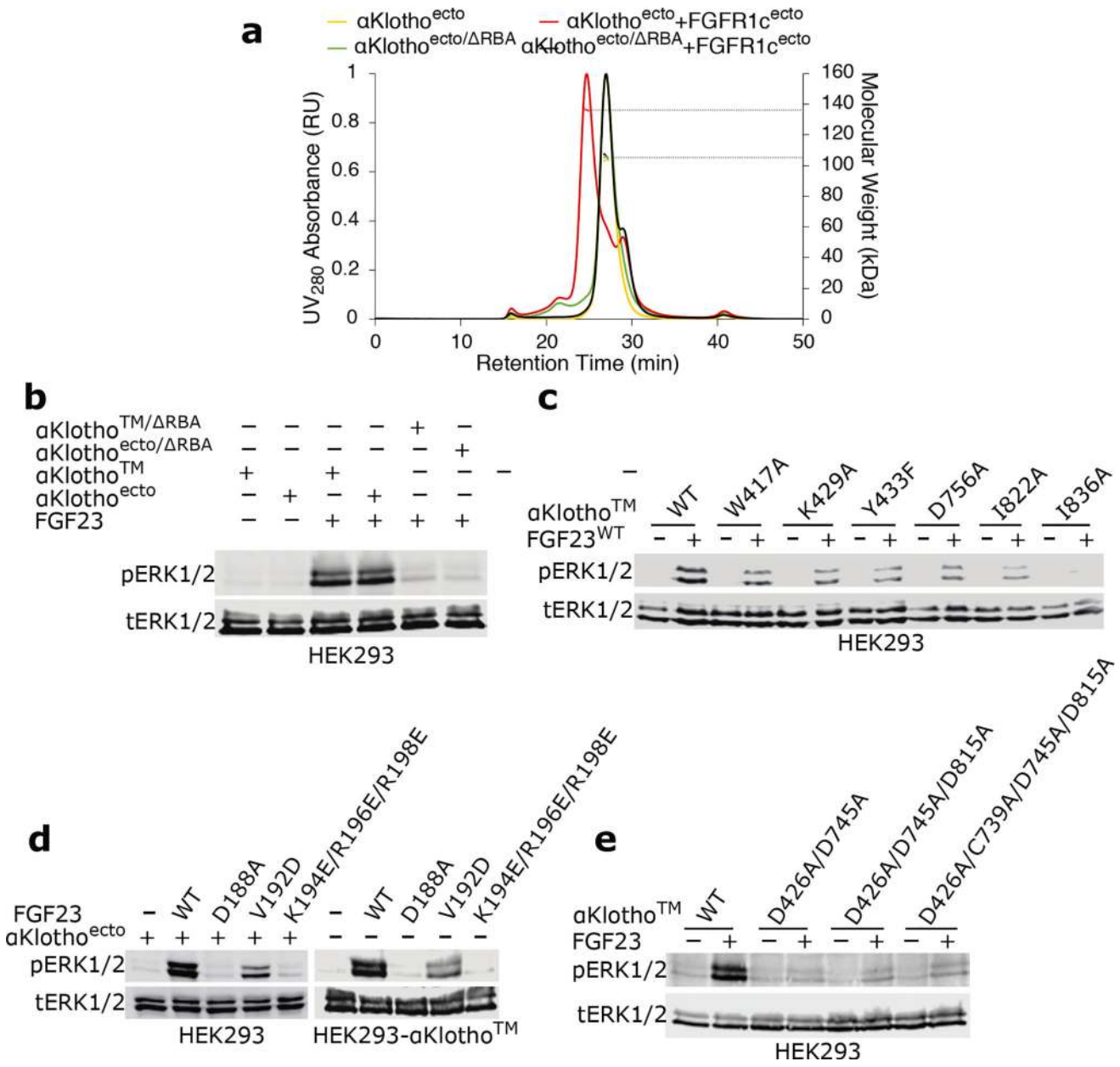

Figure 4.

Mutagenesis experiments validate the crystallographically-deduced mode of ternary complex formation. (**a**) SEC-MALS analysis of FGFR1c^{ecto} interaction with wild-type αKlotho^{ecto} or its RBA deletion mutant. RU, relative units. (**b–e**) Representative immunoblots of phosphorylated ERK (upper panels) and total ERK (lower panels, done as sample loading controls) in total HEK293 cell lysates (n=3 independent experiments for each panel). (**b**) Analysis of the effects of RBA deletion on the co-receptor activity of αKlotho^{ecto} and αKlotho^{TM} isoforms. (**c**) Analysis of mutations in the αKlotho binding pocket that engages the FGF23$^{C\text{-}tail}$. (**d**) Analysis of mutations in the FGF23$^{C\text{-}tail}$ that disrupt αKlotho–FGF23$^{C\text{-}tail}$ interaction. (**e**) Analysis of mutations of the four Zn^{2+}-coordinating amino acids in αKlotho.

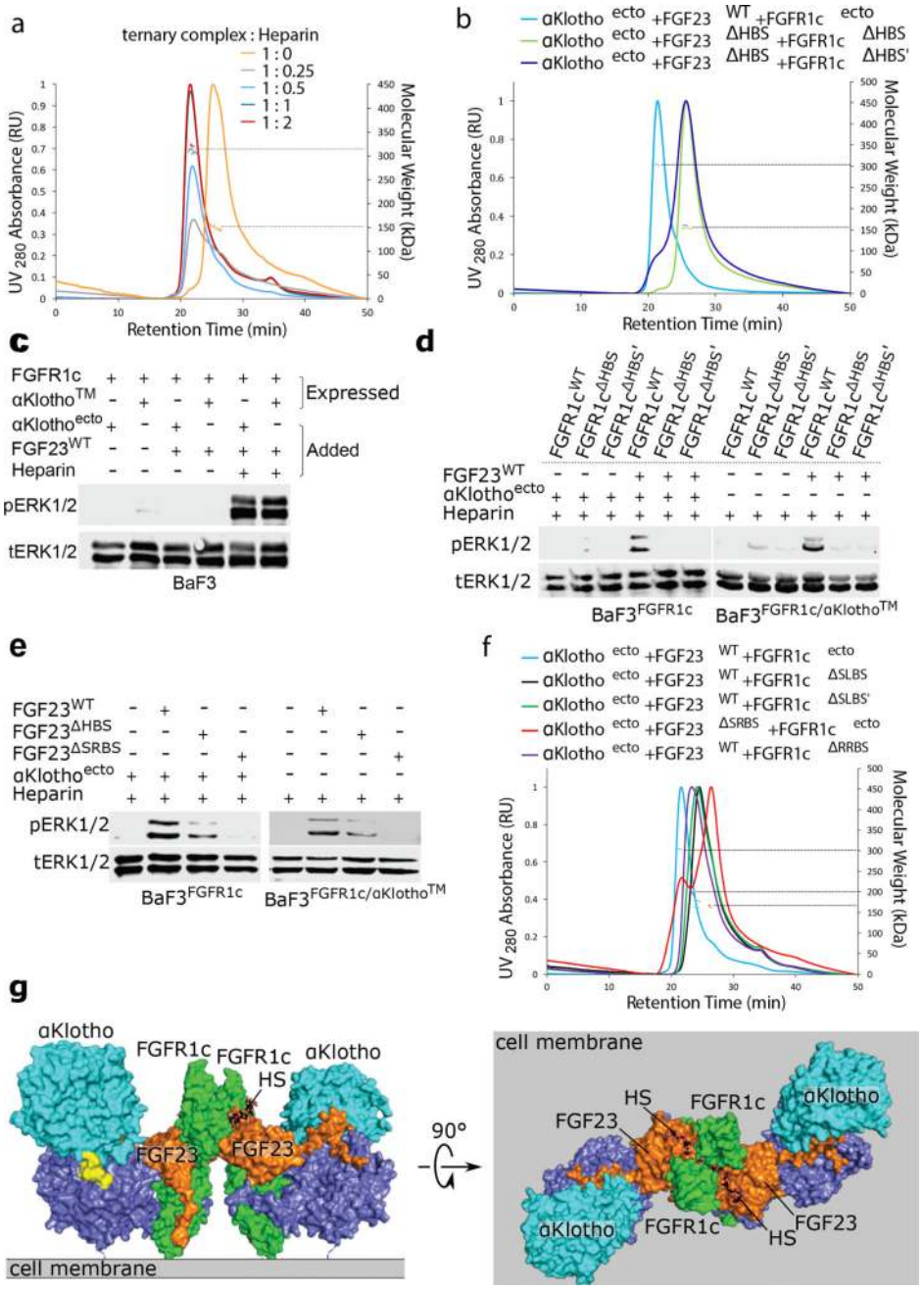

Figure 5.

HS dimerizes two 1:1:1 FGF23-FGFR1c-αKlotho complexes into a symmetric 2:2:2:2 FGF23-FGFR1c-αKlotho-HS signal transduction unit. (**a**) SEC-MALS analysis of FGF23-FGFR1c^{ecto}-αKlotho^{ecto} complex in the absence or presence of heparin hexasaccharide (HS6) present at various molar ratios. (**b**) SEC-MALS analysis of FGF23-FGFR1c^{ecto}-αKlotho^{ecto} complexes containing HS-binding site mutations of FGF23 and FGFR1c. (**c–e**) Representative immunoblots of phosphorylated ERK (top panels) and total ERK (bottom panels; sample loading controls) in total BaF3 cell lysates (n=3 independent experiments for each panel). (**c**) Analysis of HS dependency of FGF23 signaling. (**d, e**) Analysis of

mutations in the HS-binding site of FGFR1c (**d**) and in the HS-binding site or secondary receptor-binding site of FGF23 (**e**). (**f**) SEC-MALS analysis of FGF23-FGFR1c^{ecto}-αKlotho^{ecto} complexes containing a secondary receptor-binding site mutation in FGF23, a secondary ligand-binding site mutation in FGFR1c, or a direct receptor-receptor binding site mutation in FGFR1c. In (**b**) and (**f**), wild-type ternary complex served as controls. (**g**) Molecular surface of a 2:2:2:2 FGF23-FGFR1c-αKlotho-HS dimer in two orientations related by a 90° rotation around the horizontal axis: a side-view looking parallel to the plane of a cell membrane (left) and a bird's-eye view looking down onto the plane of a cell membrane (right). HS molecules are shown as black sticks.